The Bacterial Quorum-Sensing Signal 2-Aminoacetophenone Rewires Immune Cell Bioenergetics through the PGC-1α/ERRα Axis to Mediate Tolerance to Infection

Arijit Chakraborty[1,2,3#], Arunava Bandyopadhaya[1,2,&#], Vijay K Singh[1,2], Filip Kovacic[1,3,4], Sujin Cha[1], William M. Oldham[5], A. Aria Tzika[1,2], and Laurence G Rahme[1,2,3*]

[1]Department of Surgery, Massachusetts General Hospital, and Harvard Medical School, Boston, Massachusetts, USA

[2]Shriners Hospitals for Children Boston, Boston, Massachusetts, USA

[3]Department of Microbiology, Harvard Medical School, Boston, Massachusetts, USA

[4]Institute of Molecular Enzyme Technology, Heinrich Heine University Düsseldorf, Forschungszentrum Jülich GmbH, Jülich, Germany

[5]Department of Medicine, Brigham and Women's Hospital and Harvard Medical School, Boston, Massachusetts, USA

[&] Present Address: Astellas Pharma Inc., USA

[#]These authors contributed equally

[*]**Corresponding author:** Laurence G. Rahme, Ph.D

e-mail: rahme@molbio.mgh.harvard.edu (LGR)

Address: 340 Their Research Building, 50 Blossom Street, Massachusetts General Hospital, Boston, MA 02114

Phone: 617-724-5003

Author Contributions:

Author contributions: L.G.R. conceptualization, A.B., A.C. and L.G.R., designed research; A.B., A.C. V.K.S., S.H.W., S. C., performed research; A.B., A.C. V.K.S., F.K., and L.G.R. analyzed data; W.M.O and A.A.T., provided resources, and F.K. and L.G.R. wrote the paper.

Competing Interest Statement:

L.G.R. has a financial interest in Spero Therapeutics, a company developing therapies to treat bacterial infections. L.G.R.'s financial interests are reviewed and managed by Massachusetts General Hospital and Partners Health Care in accordance with their conflict-of-interest policies. No funding was received from Spero Therapeutics, and it had no role in study design, data collection, analysis, interpretation, or the decision to submit the work for publication. The remaining authors declare no competing interests.

Classification:

Biological, health, and Medical Sciences/Microbiology

Keywords: Pseudomonas aeruginosa, quorum sensing, infection, macrophages, bacterial persistence, 2-aminoacetophenone (2-AA), MvfR, PqsR, immunometabolism, host tolerization, histone deacetylation, epigenetic reprogramming, metabolic reprogramming, oxidative phosphorylation, pyruvate, mitochondrial pyruvate carrier (MPC1), peroxisome proliferator-activated receptor gamma co-activator 1-alpha (PGC-1α), estrogen-related receptor (ERRα), acetyl-CoA, ATP, bioenergetics.

Abstract

How bacterial pathogens exploit host metabolism to promote immune tolerance and persist in infected hosts remains elusive. To achieve this, we show that *Pseudomonas aeruginosa (PA),* a recalcitrant pathogen, utilizes the quorum sensing (QS) signal 2-aminoacetophenone (2-AA). Here, we unveil how 2-AA-driven immune tolerization causes distinct metabolic perturbations in macrophages' mitochondrial respiration and bioenergetics. We found that the 2-AA tolerization impairs oxidative phosphorylation (OXPHOS), leading to decreased generation of the crucial energy metabolite ATP and histone acetylation acetyl-CoA. We provide evidence that these effects result from reduced pyruvate flux into mitochondria due to the decreased expression of the mitochondrial pyruvate carrier (MPC1) mediated *via* the reduced expression and nuclear presence of its transcriptional regulator estrogen-related nuclear receptor (ERRα), leading to the weaker binding of ERRα to *MPC1* promoter. This is the outcome of the hampered interaction of ERRα with the peroxisome proliferator-activated receptor gamma coactivator 1-alpha (PGC-1α) that ultimately leads to reduced pyruvate flux into mitochondria and ATP production in tolerized macrophages. Exogenously added ATP in 2-AA exposed macrophages restores the transcript levels of *MPC1* and *ERR-α and* enhances cytokine production and intracellular bacterial clearance. Consistent with the *in vitro* findings, murine infection studies corroborate the 2-AA-mediated long-lasting decrease in ATP and acetyl-CoA and its association with PA persistence, further supporting this QS signaling molecule as the culprit of the host bioenergetic impairment and *PA* persistence. These findings unveil 2-AA as a negative modulator of cellular immunometabolism implicating the PGC-1α/ERRα axis in its influence on MPC1/OXPHOS-dependent energy production and *PA* clearance. These findings shed light on the underlying mechanisms of host tolerance and on potential therapeutic strategies to combat persistent *PA* infections.

Introduction

Host tolerance is a fundamental mechanism of innate immunity. Studies have shown that innate immune cells following infection or exposure to microbial products may enter a state of immune tolerance characterized by reduced responsiveness towards microbial re-exposure a few hours later [1-3]. Epigenetic and signaling-based mechanisms have been proposed to be involved in host immune tolerance [1-3]. In recent years, several reports have highlighted the complex interplay between metabolic reprogramming and immunity [4, 5]. It was suggested that specific metabolic programs are activated in monocytes and macrophages upon exposure to infection and microbial products [6, 7]. However, in host tolerance, the molecular mechanisms underlying immunometabolic reprogramming mediated by bacterial pathogens remain poorly understood.

Metabolic pathways are essential for generating energy for various cellular functions, including those performed by immune cells [8, 9]. Macrophages use metabolic pathways to generate energy and metabolites to adapt to changing environments and stimuli, thereby enabling them to cope with the needs of a fluctuating immune response [7, 10]. Thus, properly functioning metabolic pathways are vital for immune cells to counteract pathogens. For instance, the crucial energy-carrying molecule adenosine triphosphate (ATP) is required to phagocytose pathogen-derived molecules efficiently.

Pseudomonas aeruginosa (PA), a recalcitrant ESKAPE (*Enterococcus faecium, Staphylococcus aureus, Klebsiella pneumoniae, Acinetobacter baumannii, PA,* and *Enterobacter sp.*) pathogen, secretes virulence-associated low molecular weight signaling molecules, several of which are regulated by quorum sensing (QS) [11-14] and able to modulate host immune responses [15-18]. QS is a cell density-dependent signaling system bacteria use to synchronize their activities [11-14]. MvfR (a.k.a. PqsR), a critical QS transcription factor of *PA,* regulates the synthesis of many small molecules, including signaling molecules such as 2-aminoacetophenone (2-AA) [11, 19-21]. *In vivo* studies have demonstrated that 2-AA enables *PA* to persist in infected murine tissues by promoting innate

immune tolerance through histone deacetylase 1 (HDAC1)-mediated epigenetic reprogramming [17, 18]. 2-AA tolerization reprograms the host inflammatory signaling cascade by maintaining chromatin in a "silent" state through increased HDAC1 expression and activity and decreased histone acetyltransferase (HAT) activity [18]. These changes also impact the protein-protein interaction between HAT and cyclic AMP response element-binding protein/HDAC1 and p50/p65 nuclear factor (NF)-κB subunits [18, 22]. The 2-AA-mediated tolerization permits *PA* to persist in infected tissues [17, 18] underscoring the difference from lipopolysaccharide (LPS)-mediated tolerization, which instead leads to bacterial clearance and involves different HDACs [23].

Mitochondria, the “powerhouse” of the cells, are crucial for the regulation, differentiation, and survival of macrophages and other immune cells [8]. Our group's previous *in vivo* and *in vitro* studies indicated that 2-AA affects metabolic functions in skeletal muscle, which contains a high concentration of mitochondria [24-26]. Injection of 2-AA in murine skeletal muscle dampens the expression of genes associated with OXPHOS and the master regulator of mitochondrial biogenesis peroxisome proliferator-activated receptor-γ coactivator-1 beta (PGC-1β) [24]. Another *PA* QS molecule, 3-oxo-C12-HSL, attenuates the expression of PGC-1α [27]. PGC-1α and PGC-1β belong to the PPARγ family of inducible transcriptional coactivators and are known regulators of mitochondrial metabolism [28]. The coactivator PGC-1 proteins are involved in various cellular energy metabolic processes [29, 30], including but not limited to mitochondrial metabolism [31]. Recent studies have also emphasized the role of estrogen-related nuclear receptor α (ERRα) in coordinating metabolic capacity with energy demand in health and disease [32]. PGC-1α activates ERRα transcriptional activity through protein-protein interaction, which enhances the expression of ERRα [33, 34] and other mitochondrial genes involved in lipid metabolism and OXPHOS [35]. PGC-1α/ERRα axis has been extensively studied in cancer and established as a central regulatory node of energy metabolism that induces the global expression of genes involved in mitochondrial biogenesis and functions [36-38]. ERRα has been shown to occupy the promoter regions of many genes

119 participating in the TCA cycle and OXPHOS [39, 40], including the mitochondrial pyruvate
120 carrier (MPC1). In human renal carcinoma cells, PGC-1α/ERRα interaction results in efficient
121 activation of MPC1 expression and transport of pyruvate into mitochondrion for efficient
122 OXPHOS and energy production [41].
123 Given that our previous studies pointed to the 2-AA effect on mitochondrial functions [24-26]
124 and that mitochondria are crucial for the regulation, differentiation, and survival of
125 macrophages and other immune cells [8] we investigated how 2-AA may mediate cellular
126 metabolic reprogramming in tolerized immune cells by examining the link between the PGC-
127 1α/ERRα axis and 2-AA-mediated immune tolerance. Our findings uncovered the crucial action
128 of 2-AA on energy homeostasis and metabolism in tolerized immune cells through
129 perturbances of the ERRα/PGC-1α interaction, MPC1-mediated pyruvate transport and the
130 production of the key energy metabolism molecules, ATP and acetyl-CoA and their association
131 with the persistence of *PA* in mammalian tissues.
132
133
134 **Results**
135 **Tolerization by 2-AA impacts the generation of crucial energy metabolites in**
136 **macrophages**

137 Following infection or exposure to microbial products, innate immune cells may enter
138 a state of tolerance several hours later, as depicted by their diminished responsiveness or
139 unresponsiveness to microbial re-exposure [1-3, 42]. Given that 2-AA tolerized cells are non-
140 responsive to 2-AA re-exposure, we investigated the impact of 2-AA on energy homeostasis
141 and metabolism in non-tolerized and tolerized BMDM cells (Fig. 1). We quantified the levels of
142 ATP and acetyl-CoA, which is a fuel for ATP production, in a series of *in vitro* experiments in
143 which murine BMDM cells were exposed to 2-AA (1st 2-AA exposure) or re-exposed (2nd 2-AA
144 exposure) to respectively determine their activation, and tolerance as well as memory to this

145 QS molecule (Fig. 1A). Initially, following the 1st 2-AA exposure (black bars), a significant
146 increase in the concentrations of intracellular ATP (Fig. 1B) and acetyl-CoA (Fig. 1C) was
147 observed in BMDM cells exposed to 2-AA for 1 and 6 h compared to their corresponding naïve
148 control cells (grey bars). However, cells exposed to 2-AA for 48 h (black bar) appeared to have
149 entered a state of tolerance as ATP and acetyl-CoA levels were decreased compared to 2-AA
150 exposures for a shorter time (Figs. 1B and 1C). The tolerance of these cells as well as their
151 memory to 2-AA was determined by their responsiveness to a 2nd 2-AA exposure (Fig. 1A). To
152 achieve this, these cells were washed to remove 2-AA and allowed to rest for 24 or 106 h in
153 the absence of 2-AA before receiving the 2nd 2-AA exposure for 1 or 6 h (Fig. 1A). Figures 1B
154 and 1C (red bars) show the unresponsiveness of BMDM cells to 2-AA re-exposure as
155 evidenced by the similar levels of ATP and acetyl-CoA compared to cells exposed to 2-AA for
156 48 h (1st exposure black bars). The sustained unresponsiveness of the cells to re-exposure
157 indicates that the cells exhibited innate immunological memory, which could not be reverted
158 by 2-AA re-exposure. Similar responsiveness patterns of ATP and acetyl-CoA as with BMDM
159 cells were observed in murine macrophage RAW 264.7 cells (Figs. S1A and S1B) or human
160 monocyte THP-1 cells (Figs. S1C and S1D) following exposure or re-exposure to 2-AA. These
161 findings further support our observations with BMDM cells and confirm that either cell type can
162 be used to study responses to 2-AA. These results reinforce the notion that 2-AA impacts
163 crucial energy metabolites in macrophages.

164 Moreover, we sought to determine whether 2-AA-tolerized BMDM cells would respond
165 to heterologous stimulus. To test this, we re-exposed the cells to lipopolysaccharide (LPS), an
166 outer membrane bacterial component that strongly induces macrophages. LPS re-exposure of
167 the 2-AA tolerized BMDM cells did not significantly (p = 0.9) increase ATP levels (Fig. S2),
168 indicating that 2-AA cross-tolerized the cells to this heterologous bacterial immunostimulant.
169 On the other hand, as expected, we observed increased ATP levels following LPS stimulation
170 of the non-tolerized BMDM cells (Fig. S2). The broad spectrum of 2-AA cross-tolerization

171 strongly suggests an interplay of epigenetic mechanism rather than ligand-receptor mediated
172 signaling-based mechanism in bringing out the observed 2-AA-mediated tolerance.

173 **Tolerization by 2-AA leads to a quiescent state by reducing cell bioenergetics and**
174 **compromising OXPHOS.**

175 To further investigate the 2-AA's impact on the bioenergetics of macrophages, we
176 assessed by Seahorse assay the oxygen consumption rate (OCR) as an index of OXPHOS
177 in 2-AA exposed (for 1 and 24 h) and re-exposed (2nd exposure for 1 h) BMDM cells (Fig. 1D).
178 Values of basal (Fig. 1E) and maximal (Fig. 1F) mitochondrial respiration and spare
179 respiratory capacity (Fig. S3) interpreted from these measurements revealed that 1 h 2-AA
180 exposure of naïve cells significantly increased OCR compared to naïve control cells. At 24 h
181 post-2-AA exposure, cells had a significantly reduced basal OCR level than the control BMDM
182 cells, indicating decreased OXPHOS and an overall quiescent phenotype of tolerized
183 macrophages. Re-exposure of tolerized macrophages with 2-AA also did not augment
184 maximal and basal OCR (Figs. 1D-1F), indicating the unresponsiveness of tolerized BMDM
185 cells.

186 These OCR data are consistent with previous direct measurements of ATP (Fig. 1B)
187 and acetyl-CoA (Fig. 1C) and support the notion that 2-AA tolerization induces a quiescent
188 phenotype in these cells characterized by defective OXPHOS. These findings confirm that 2-
189 AA mediates energy homeostatic and metabolic alterations in the immune cells and that 2-AA
190 tolerization arrests these cells in a sustained 2-AA-unresponsive state.

191 **The pyruvate transport into mitochondria is decreased in tolerized macrophages.**

192 Since acetyl-CoA and ATP levels were reduced due to 2-AA tolerization, we
193 investigated whether the mitochondrial dysfunction observed is related to pyruvate
194 metabolism. Pyruvate links glycolysis with mitochondrial production of acetyl-CoA and ATP *via*
195 the tricarboxylic acid (TCA) cycle and OXPHOS [7]. RAW 264.7 cells initially exposed to 2-AA

196 for 1 or 3 h (black bars) exhibited significantly higher concentrations of cytosolic and
197 mitochondrial pyruvate compared to the corresponding naïve control cells (Fig. 2A). Pyruvate
198 significantly decreased over time in cytosolic and mitochondrial fractions as cells were entering
199 into the tolerized state (Fig. 2A). Tolerized cells remain unresponsive to 2-AA re-exposure (red
200 bars), exhibiting no significant change in the concentration of pyruvate in the cytosolic or
201 mitochondrial fraction (Fig. 2A). A similar result was observed in THP-1 cells (Figs. S1E and
202 S1F).

203 To gain a better understanding of the 2-AA-mediated reductions in mitochondrial
204 pyruvate, ATP production, and acetyl-CoA levels, we sought to determine the involvement of
205 the MPC1 [41] that is crucial in transporting pyruvate from the cytosol into the mitochondria
206 [43]. Western blot studies of whole cell lysates of RAW 246.7 cells exposed to 2-AA showed a
207 significant decrease over time in the abundance of MPC1 protein, and tolerized cells remain
208 unresponsive to 2-AA re-exposure (Fig. 2B). Together these findings suggest that 2-AA
209 tolerization dysregulates MPC1 mediated transport of the pyruvate into mitochondria.

210

211 **2-AA tolerization suppresses ERRα binding to the *MPC1* promoter and the interaction**
212 **between PGC-1α and ERRα**

213 Given that the PGC-1α/ERRα axis is the transcriptional regulatory node that activates
214 the expression of MPC1 [33] we determined the protein levels of ERRα. Western blot studies
215 of whole cell lysates showed a significant decrease over time in the abundance of ERRα
216 protein following 1st exposure of RAW 246.7 cells to 2-AA, while tolerized cells remain
217 unresponsive to 2-AA re-exposure (Fig. 3A). By assessing the cytosolic and nuclear
218 abundance of ERRα in tolerized cells we found that both fractions had lower levels of ERRα
219 protein than their corresponding control cells (Fig. 3B).

220 Furthermore, because an ERRα binding putative DNA motif (TNAAGGTCA) has been
221 identified upstream of the *MPC1* promoter in humans [41], and we found the same motif to be

222 present 1.5 kB upstream of the transcription start site of mouse *MPC1* promoter, we analyzed
223 if tolerization led to reduced ERRα binding to the *MPC1* promoter motif TNAAGGTCA.
224 Chromatin immunoprecipitation (ChIP) assay followed by qPCR analysis revealed that in
225 tolerized cells, ERRα binds approximately 4-fold less efficiently to the putative binding site on
226 the *MPC1* than in corresponding control cells (Fig. 3C).
227 Since the transcriptional activity of ERRα is regulated through a protein-protein interaction with
228 the transcriptional coactivator PGC-1α [33] we assessed whether the formation of the PGC-
229 1α/ERRα complex is affected in 2-AA tolerized cells. Using paraformaldehyde fixed nuclear
230 lysates of RAW 264.7 tolerized and naïve cells, we performed a co-immunoprecipitation (co-
231 IP) of PGC-1α and reverse co-IP with ERRα followed by immunoblotting (Fig. 3D). As shown
232 in Figure 3D less ERRα was detected when PGC-1α was pulled down in presence of 2-AA
233 than in naïve control cells. Moreover, reverse co-IP with ERRα protein showed lower levels of
234 PGC-1α in the presence of 2-AA than in naïve control cells (Fig. 3D). Control IgG showed no
235 detectable levels of ERRα following nuclear fraction pull down. These results indicate that in
236 the tolerized macrophages, PGC-1α/ERRα interaction is impaired (Fig. 3D).
237 Since PGC-1α enhances the transcriptional activity of ERRα through their interaction,
238 and ERRα transcription is regulated *via* an autoregulatory loop [34], we examined the effect of
239 tolerization on the transcription of *ERRα* and its target gene *MPC1*. Using RAW 264.7 cells
240 infected with the wild type *PA* strain PA14 or isogenic Δ*mvfR* mutant, which does not produce
241 2-AA [21] we observed lower RNA transcript levels of *MPC1* (Fig. 4A) and *ERRα* (Fig. 4B) in
242 PA14 compared to Δ*mvfR*. The addition of 2-AA to Δ*mvfR* decreased the levels of both gene
243 transcripts to the levels similar to PA14 infection condition, supporting the role of 2-AA in effect.
244 To test if the observed effects are due to MPC1 dependent reduction of mitochondrial ATP
245 generation, we supplemented the macrophages with ATP. The findings indicate that the
246 addition of ATP in PA14 infected cells elevated the transcript levels of both *ERRα* and *MPC1*,
247 but not in the Δ*mvfR* infected macrophages (Fig. 4A and 4B). These results indicate that

248 reduced MPC1 function is due to negative effect of 2-AA tolerization on the transcriptional
249 activation of *MPC1* through PGC-1α/ERRα axis.
250
251 **2-AA tolerization impairs macrophage-mediated intracellular bacterial clearance**
252 **through decrease in MPC1-mediated pyruvate import, ATP, and TNF-α levels.**

253 2-AA-mediates persistence of *PA in vivo,* dampens proinflammatory responses and
254 increases the intracellular burden of this pathogen in macrophages *via* epigenetic
255 modifications [17, 18, 26]. Here we used RAW 264.7 cells that were infected with the PA14 or
256 the 2-AA deficient Δ*mvfR* mutant to assess the clearance of *PA* by macrophages.
257 Macrophages infected with PA14 showed increased bacterial burden than the cells infected
258 with Δ*mvfR,* and 2-AA supplementation to Δ*mvfR* lead to increase bacterial burden (Fig. 4C).
259 Furthermore, we used UK5099 and ATP to interrogate whether MPC1 mediated mitochondrial
260 pyruvate import and bioenergetics are linked to the clearance of *PA* intracellular burden. The
261 addition of the UK5099 inhibitor strongly enhanced the bacterial intracellular burden in Δ*mvfR*
262 infected macrophages compared to the non-inhibited cells (Fig. 4C). UK5099 had no effect on
263 PA14 infected macrophages. Conversely, exogenously added ATP to macrophages infected
264 with PA14 strongly reduced the *PA* intracellular and had no change Δ*mvfR* infected cells (Fig.
265 4C).
266 Given that 2-AA tolerization decreases the expression of pro-inflammatory cytokine
267 TNF-α by hypo-acetylating the core histone 3 lysine 18 acetylation (H3K18ac) mark at TNF-α
268 promoter [18], we investigated the link between bioenergetics and TNF-α expression in
269 infected macrophages. UK5099, or ATP was added exogenously to infected macrophages with
270 PA14 or Δ*mvfR* (Fig. 4D). As shown in Figure 4D, PA14 infected cells showed lower TNF-α
271 transcript levels compared to the Δ*mvfR* infected cells. Supplementation of 2-AA to Δ*mvfR*
272 infected cells led to decrease in the TNF-α transcript levels. Moreover, the addition of the MPC1
273 inhibitor, UK5099 in Δ*mvfR* infected counteracted the increase in TNF-α transcript levels, while

274 had no effect in PA14 infected macrophages (Fig. 4D). Conversely, exogeneous addition of
275 ATP to PA14 infected cells enhanced the transcription of TNF-α compared to the untreated
276 PA14 infected cells, while no changes in TNF-α expression levels were observed in Δ*mvfR*
277 infected macrophages (Fig. 4D).

278 These findings strongly suggest that 2-AA tolerization severely impairs macrophages'
279 ability to facilitate the clearance of *PA* intracellular burden, *via* mechanism which involves
280 reduction in MPC1-mediated pyruvate import into mitochondria, ATP levels and TNF-α
281 transcription.

282 ***In vivo* studies corroborate the 2-AA-mediated decrease *in vitro* of the central metabolic**
283 **fuel acetyl-CoA and the energy-carrying molecule ATP and their association with *PA***
284 **persistence.**

285 To determine whether the decrease in the key metabolites mediated by 2-AA is also
286 observed *in vivo* during infection, we quantified the levels of ATP and acetyl-CoA in murine
287 spleen tissues at 1, 5, and 10 days (Fig. 5). This organ was selected for our immunometabolic
288 studies due to its role in regulating not only local but also systemic (whole-body) immune
289 responses, facilitated by various immune cells including macrophages [44]. Mice were infected
290 with *PA* strain PA14, or isogenic mutant Δ*mvfR,* which does not produce 2-AA [21]. It is
291 important to note that it is not possible to generate or utilize a bacterial mutant that is defective
292 in 2-AA only because 2-AA is formed by spontaneous decarboxylation rather than by an
293 enzyme-catalyzed reaction [45-47]. Therefore, animals that were either infected with Δ*mvfR*
294 and received 2-AA (Δ*mvfR*+2-AA) at the time of infection or uninfected mice injected with a
295 single dose of 2-AA served as direct controls (Fig. 5). Naïve and sham mice groups served as
296 additional basal controls (Fig. 5).

297 Infection with PA14 or uninfected mice injected with 2-AA led to a significant decrease
298 in both ATP (Fig. 5A) and acetyl-CoA (Fig. 5B) concentrations in spleen tissues compared to
299 Δ*mvfR* infected mice that sustained higher ATP and acetyl-CoA levels similar to naïve and

300 sham control groups across the time points tested. However, in mice infected with Δ*mvfR* and
301 2-AA injected *(*Δ*mvfR*+2-AA) at the time of infection, ATP and acetyl-CoA concentrations in the
302 spleen decreased to levels comparable to those of PA14-infected animals, strongly indicating
303 the biological function of 2-AA in decreasing these key metabolites. These *in vivo* findings
304 further support the adverse action of 2-AA on host energy homeostasis and metabolism
305 observed *in vitro* studies.

306 The metabolic alterations observed are associated with the persistence of *PA* (Fig. 5C). Using
307 *Pseudomonas* isolation agar plates, we evaluated the bacterial load at the infection site over
308 the course of 10 days, obtaining samples at 1, 5, and 10 days. At one day post-infection, mice
309 infected with PA14, Δ*mvfR,* or Δ*mvfR*+2-AA exhibited no difference in bacterial burden (Fig.
310 5C), verifying the ability of all strains to establish infection. At 5- and 10-days post-infection,
311 mice infected with PA14 or Δ*mvfR*+2-AA sustained the bacterial burden at a significantly higher
312 bacterial burden over time compared to those infected with Δ*mvfR* (Fig. 5C). These results are
313 consistent with our previous findings [17, 18] and provide compelling evidence that the
314 metabolic alterations identified may favor *PA* persistence in infected tissues.

315 **Discussion**

316 The *PA* signaling molecule 2-AA that is abundantly produced and secreted in human tissues
317 [21, 22] is the first QS molecule that epigenetically reprograms immune functions, promotes
318 immune tolerance, and sustains *PA's* presence in host tissues [17, 18, 22, 26]. The present
319 study provides insights into the mechanistic actions of 2-AA on cellular metabolism that
320 contribute to host immune tolerance to infection. We uncover that this signaling molecule
321 causes distinct metabolic alterations in macrophages' mitochondrial respiration and energy
322 production promoted via the PGC-1α/ERRα axis and MPC1-dependent OXPHOS that links
323 the TCA cycle to the production of ATP and energy homeostasis (Fig. 6). Our results show that
324 2-AA tolerization decreases ATP the crucial energy metabolite and the histone acetylation
325 metabolite acetyl-CoA and *in vivo*, implicating the importance of the key energy-producing

326 mitochondrial process in immune tolerance. Although macrophages respond to the first
327 exposure to 2-AA by enhancing ATP and acetyl-CoA production, long-term exposure to 2-AA
328 leads to a tolerized state characterized by sustained reduced ATP and acetyl-CoA
329 concentrations, a quiescent bioenergetic state with reduced pyruvate flux and
330 unresponsiveness to a 2nd exposure.

331 Our results reveal that the decrease of ATP and acetyl-CoA in tolerized macrophages
332 results from the 2-AA-mediated perturbation of the physical interaction between ERRα and
333 PGC-1α. The PGC-1α/ERRα axis has not previously been implicated in tolerization but has
334 been extensively studied in cancer, underscoring the novelty of our findings. Studies in cancer
335 cells have shown that the physical interaction of human ERRα with PGC-1α strongly enhances
336 the binding of ERRα to DNA to induce the activation of the targeted genes [33] including *MPC1,*
337 responsible for the import of cytosolic pyruvate into mitochondria and PDH, that catalyzes the
338 conversion of pyruvate to acetyl-CoA. Inhibition of ERRα has been shown in cancer cell
339 metabolism studies to interfere with pyruvate entry in mitochondria by inhibiting the expression
340 of MPC1 [48]. Indeed, we find that the transcription of *ERRα* and *MPC1* genes and pyruvate
341 entry into mitochondria is reduced in tolerized macrophages. Given that pyruvate is a primary
342 carbon source in the TCA cycle that fuels OXPHOS and the production of ATP into
343 mitochondria, it explains the reduced ATP and acetyl-CoA levels observed in tolerized
344 macrophages. Future studies will focus on unveiling the pathways by which macrophages
345 respond to the bioenergetic changes identified and decipher their effect on pyruvate cycle in
346 host tolerance to infection [49-51].

347 We show that the unprecedented action of a QS bacterial small signaling molecule on
348 the interaction between ERRα and PGC-1α in the nucleus is hampered. Although it remains to
349 be elucidated whether 2-AA interferes directly or indirectly on the PGC-1α/ERRα axis, our data
350 bring up the possibility that the reduced production of acetyl-CoA may be responsible, since
351 cholesterol is a known coactivator/ligand of ERRα [52] is generated from acetyl-CoA [52]. This
352 possibility may also explain the reduced expression of *ERRα* and its lower abundance since

353 cholesterol is also required for its activation and autoregulation. However, it is also possible
354 that 2-AA may antagonize the interaction between ERRα and PGC-1α by binding to ERRα.
355 Small molecules as antagonist of ERRα have been reported previously [53]. The weaker
356 binding of ERRα to the *MPC1* promoter site, and consequently reduced MPC1 expression
357 explains the reduced pyruvate presence in mitochondria and that of ATP and mitochondrial
358 quiescence.

359 The observed cellular metabolic perturbances also align with our previous studies in
360 skeletal muscle, which pointed to mitochondrial dysfunction triggered by 2-AA [24, 25].
361 Interestingly, the *PA* QS LasR-regulated homoserine lactone molecule, 3-oxo-C12-HSL, was
362 reported to attenuate the expression of PGC-1α and decreasing the mitochondrial respiratory
363 capacity [27] and promoting apoptosis in lung epithelial cells [54]. Moreover, another *PA* QS
364 molecule PQS also regulated by LasR was recently shown to induce organelle stress, including
365 mitochondria, by disrupting the mitochondrial membrane potential in human macrophages [55].
366 As opposed to 2-AA, which dampens the pro-inflammatory response, PQS increases
367 proinflammatory cytokines [55], consistent with the fact that PQS is an acute infection type
368 molecule unrelated to chronic/persistent infections.

369 Previously, we reported that 2-AA tolerization induces HDAC1 expression and activity,
370 reducing H3K18ac at the TNF-α promoter [18]. The findings with TNF-α transcription using
371 UK5099 and ATP in 2-AA treated macrophages are in support of the bioenergetics
372 disturbances observed in macrophages and their link to epigenetic modifications we have
373 shown to be promoted by 2-AA [18]. Macrophages exposed to 2-AA in the presence of
374 exogenous ATP showed improved intracellular bacterial clearance and enhanced TNF-α
375 levels, supporting the epigenetic interconnection of macrophages and cellular ATP
376 responsiveness levels against infection. The exogenous addition of UK5099 that reverted the
377 efficiency of the *mvfR* infected macrophages to clear the *PA* intracellular burden and the

378 counteraction to the 2-AA effect by ATP addition that increases the clearance of *PA* intracellular
379 burden support the importance of this energy-carrying molecule in *PA* persistence.

380 The results with the MPC1 inhibitor, UK5099, suggest that the availability of pyruvate
381 could underlie the mechanism of 2-AA-regulated HDAC/HAT-dependent control of transcription
382 of pro-inflammatory mediators and bacterial clearance [56]. These results align with our
383 previous findings, showing that establishing bacterial intracellular burden in macrophages is
384 HDAC1 dependent [56]. It remains to be elucidated if HDAC/HAT-mediated histone
385 modification directly regulates expression of OXPHOS genes in 2-AA tolerized macrophages
386 as it was shown that histone deacetylation downregulates OXPHOS in persistent *M.*
387 *tuberculosis* infection [57, 58]. Given the complexity of 2-AA-mediated long-term effects, future
388 omics studies combined with immune profiling may aid in deciphering the possible network of
389 co-factors across different subpopulations of immune cells and the immunometabolic
390 reprogramming related to 2-AA.

391 We have shown that although 2-AA tolerization leads to a remarkable increase in the
392 survival rate of infected mice, it permits an HDAC1-dependent sustained presence of *PA* in
393 mice tissues and intracellularly in macrophages [17, 18, 22, 26]. Here, we use 2-AA-producing
394 and isogenic non-producing *PA* strains to confirm the 2-AA-mediated decrease in the central
395 metabolite acetyl-CoA and the energy-carrying molecule ATP during infection. These murine
396 infection studies provide strong evidence of the 2-AA biological relevance in reducing these
397 metabolites *in vivo*. Taking together our previous and current findings, these *in vivo* studies
398 provide compelling evidence that the metabolic alterations identified may favor *PA* persistence
399 in infected tissues.

400 That 2-AA permits *PA* to persist in infected tissues despite rescuing the survival of
401 infected mice underscores its difference from that of LPS tolerization, which results in bacterial
402 clearance [23] *via* the mechanism that relies on a set of different HDAC enzymes. LPS
403 tolerization predominantly involves changes in H3K27 acetylation [59], while 2-AA tolerization

404 involves H3K18 modifications [22]. The 2-AA-mediated effects reported here are also distinct
405 from Sirtuin 1 and 6-dependent epigenetic-metabolic reprogramming mediated by LPS [60],
406 which promotes endotoxin tolerance in immune cells by upregulating glycolysis and
407 suppressing OXPHOS [61]. Although short-term exposure of BMDMs to LPS enhances ATP
408 production, we could not observe this effect in 2-AA tolerized cells.

409 Metabolic reprogramming upon infection may be pathogen-specific, with each
410 pathogen impacting specific metabolic pathways that better fit its respective metabolic needs
411 [7]. This was shown for infections of various tissues with *Chlamydia pneumonia*, *Legionella*
412 *pneumophila*, *Mycobacterium tuberculosis*, and *Salmonella* [62-65] and, by our group, for *PA*
413 infections [17, 18, 24]. It would be interesting, however, to test whether 2-AA affects the killing
414 efficacy of macrophages against other pathogens, as emerging evidence shows that
415 synergistic or antagonistic interactions between clinically relevant microorganisms and host
416 have important implications for polymicrobial infectious diseases [66].

417 While in this study, we focused on the role of ERRα mainly in pyruvate metabolism,
418 future studies are needed to reveal other ERRα/PGC-1α axis-dependent metabolic and
419 immune pathways are modulated by 2-AA. In this view, the cholesterol synthesis pathway that
420 relies on acetyl-CoA precursor, as cholesterol is a known coactivator/ligand of ERRα [52] and
421 fatty acid catabolism, generating acetyl-CoA, and PGC-1α regulates fatty acid oxidation [67].

422 In summary, our study highlights the role of 2-AA in orchestrating cellular metabolic
423 reprogramming in addition to the epigenetic reprogramming reported previously. This
424 immunometabolic reprogramming that ultimately leads to host tolerance favoring the prolonged
425 presence of *PA* in the infected host resembles trained immunity, a nonspecific form of immune
426 memory in which an initial exposure to a pathogen “trains” innate immune cells to respond to
427 a re-exposure differently than their unexposed counterparts with the help of epigenetic
428 changes [68, 69]. The reported immunometabolic reprogramming contributes to a better
429 understanding of the molecular and cellular mechanisms, biomarkers, and functional

430 significance that may be involved in immune tolerance to infection, providing for designing and
431 developing innovative therapeutics and interventions. These approaches can focus on
432 promoting host resilience against bacterial burden and safeguarding patients from recalcitrant
433 persistent infections.

434

435 **Materials & Methods**

436 **Ethics statement**

437 The animal protocol was approved by the Institutional Animal-Care and Use Committee
438 (IACUC) of Massachusetts General Hospital (protocol no. 2006N000093). No randomization
439 or exclusion of data points was applied.

440 **Conditions used for the exposures of the cells to 2-AA**

441 Mouse BMDM cells were isolated from femur of CD1 6 weeks old male and female mice and
442 used to estimate the levels of various metabolites (Fig. 2A) following exposure and re-exposure
443 to 2-AA (Fig. 1A). The 1st exposure of naïve BMDMs (10^6/mL in 6-well plates) was achieved
444 with 400 μM 2-AA for 1, 6, or 48 h. Cells exposed for 48 h were used for the 2nd 2-AA exposure.
445 These cells were washed to remove residual 2-AA, left in the medium in the absence of 2-AA
446 for either 24 or 106 h, and re-exposed to 2-AA (200 μM) for 1 or 6 h, respectively. For RAW
447 264.7 (10^6/mL in 6-well plates) and THP-1 cells (10^6/mL in 6-well plates) the 2-AA concentration
448 and conditions used were as with BMDM cells. The hours of the 1st round and 2nd round of
449 exposure to 2-AA are indicated in Figure S1.

450 For the LPS stimulation studies, cells were stimulated with 400 μM 2-AA or 100 ng/mL LPS for
451 6 h, and 800 μM of 2-AA for 48 h. Cells receiving 1st exposure for 48 h were washed and re-
452 exposed to 400 μM of 2-AA or 100 ng/mL LPS for 6 h.

453 **ATP and acetyl-CoA quantifications**

454 The levels of ATP, acetyl-CoA, and were assessed in BMDM and RAW264.7 macrophage cells
455 following exposure to 2-AA at the times indicated and by utilizing the ATP Assay kit
456 (cholorimetric/fluorometric) (#ab83355, Abcam) and the PicoProbe AcCoA assay kit (ab87546,
457 Abcam), respectively, according to the manufacturer's instruction. Quantifications of ATP and
458 acetyl-CoA were performed in triplicates.

459 ***ATP***: For ATP determination, macrophages were lysed and subsequently centrifuged at 14,000
460 rpm for 10 min at 4 °C. The supernatants were transferred to a fresh Eppendorf tube.
461 Standards and cell supernatants of 50 µL were added to a 96-well plate suitable for fluorescent
462 analysis (black sides, clear bottom). A reaction mixture containing an ATP converter, probe,
463 buffer, and developer mix was then added to all wells (50 µL) and incubated away from light at
464 room temperature for 30 min. ATP quantification was conducted fluorometrically at 535/587 nm
465 using a plate reader and the following settings: λex = 535 nm; λem = 587 nm. Fluorescence
466 was measured using a microplate reader (Tecan Group Ltd, Männedorf, Switzerland)

467 *Acetyl-CoA*: Acetyl-CoA content was assessed by first deproteinizing total cell fractions of
468 macrophages using the perchloric acid and then centrifuging at 14,000 rpm for 10 min at 4 °C.
469 50 µL of cells' supernatant sample CoASH were quenched to correct the background
470 generated by free CoASH. Following the homogenization procedure described above, the
471 samples were diluted with the reaction mix, and fluorescence was quantified using a plate
472 reader and the settings as above with ATP.

473 **Seahorse Assays**

474 Seahorse analysis was performed according to previously published protocols [70]. Briefly,
475 freshly prepared BMDM cells were reseeded in complete RPMI-1640 cells using Seahorse
476 plates (Agilent cat. no. 103729100) at a density of 5×10^4 cells per well. Cells were exposed
477 to 400 µM 2-AA for 1 h or 24 hours (1st exposure). Cells receiving 1st exposure for 24 h were
478 washed and re-exposed to 200 µM of 2-AA for 1 h. Naïve cells were used as control. Prior to

479 initiating Seahorse measurements cells were washed and Seahorse XF DMEM supplemented
480 with 2 mM glutamine (Gibco cat. No. 25030-081) was added to each well. Cells were allowed
481 to stabilize in a 37°C incubator without CO_2 for 1 h. The Seahorse cartridge was hydrated and
482 calibrated as per the manufacturer's instructions. The Mitochondrial stress test kit (Agilent cat.
483 no. 10395-100) was used (oligomycin at 1 μM, FCCP (1.5 μM), rotenone (0.5 μM), and
484 antimycin A at (0.5 μM)) with slight modifications according to the published protocol [70] that
485 included injection of 25 mM glucose, and sodium pyruvate (1 μM). All samples N= 4 were run
486 in a Seahorse XFe96 Analyzer, and data were analyzed using Wave and plotted using
487 GraphPad Prism software.

488 **Isolation of cytosolic and mitochondrial fraction and pyruvate quantification**

489 Pyruvate is produced in the cytosol and is transported into the mitochondria. RAW 264.7 cells
490 were plated at 1×10^6 to incubate overnight at 37°C in a CO2 incubator. Cells were exposed
491 to 2-AA for 1, 3, 24 or 48 h or re-exposed for 1 h as described above. Mitochondria and
492 cytosolic fractions of each group were isolated utilizing the Mitochondria Isolation Kit for
493 cultured cells (#ab110170, Abcam) following the manufacturer's protocol. Briefly, cells were
494 collected with a cell lifter and pelleted by centrifugation at 1,000 g, frozen, and then thawed to
495 weaken the cell membranes. The cells were resuspended in Reagent A and transferred into a
496 pre-cooled Dounce Homogenizer. The homogenates were centrifuged at 1,000 g for 10 min at
497 4°C and saved as supernatant #1 for the cytosolic fractions. The pellet was resuspended in
498 Reagent B, followed by repeat rupturing and centrifugation. The pellet was collected and
499 resuspended in 500 μL of Reagent C supplemented with Protease Inhibitor cocktails (P8340,
500 Sigma Aldrich). Following separation, a Bradford assay was conducted to determine the
501 protein concentration in each fraction. Pyruvate levels were determined in cellular fractions
502 and mitochondrial fractions by using the Pyruvate Assay Kit (#ab65342, Abcam) according to
503 the manufacturer’s instructions. Briefly, after deproteinization using perchloric acid, the
504 samples were neutralized in ice-cold 2 M KOH. 10 μL samples were incubated with reaction

505 mix and kept on the plate at RT for 30 min in the dark. The absorbance was measured in a
506 microplate reader (Tecan Group Ltd, Männedorf, Switzerland) at 570 nm and results are shown
507 from three independent experiments.

508 **Bacterial strains and growth conditions**

509 The *P. aeruginosa* strain known as Rif^R human clinical isolate UCBPP-PA14 (also known as
510 PA14) was used [71]. The bacteria were grown at 37 °C in lysogeny broth (LB) under shaking
511 and aeration or on LB agar plates containing appropriate antibiotics. PA14 and isogenic mutant
512 Δ*mvfR* [19] cultures were grown in LB from a single colony to an optical density of 600 nm
513 (OD_{600}) of 1.5, diluted 1:50,000,000 in fresh LB media, and grown overnight to an OD_{600} of 3.0.

514 **Gentamicin protection assay**

515 RAW264.7 macrophage cells were plated on 6 well cell culture-treated plates overnight in
516 pyruvate free DMEM. After 3 h of incubation with 10 μM UK5099, 20 μM ATP or 400 μM 2-AA,
517 cells were infected with PA14 and isogenic mutant *ΔmvfR* at 5 MOI for 30 min at 37 °C in 5%
518 CO2. Unbound bacteria were removed by washing once with cold DMEM medium. Afterwards,
519 the cells were incubated with 100 μg/ml of gentamicin for 30 min to eliminate residual
520 extracellular bacteria. The cells were washed with DMEM and transferred to free medium
521 without gentamicin and kept for 3 h at 37°C in 5% CO2. The infected cells were scraped after
522 3 h, centrifuged at 500 × g, and lysed in distilled water. The lysed cells were immediately diluted
523 in PBS and plated on LB agar plates to assess bacterial presence. Bacterial colony-forming
524 units (CFUs) were counted after incubating the plates overnight at 37°C.Untreated cells
525 infected with PA14 were set as 100 % and the reduction of Bacterial load was expressed as
526 %CFU.

527 **Pharmacological inhibitors and ATP supplementations**

528 For the OXPHOS inhibition assay, RAW264.7 macrophage cells were treated with UK5099 (10
529 μM, Sigma-Aldrich, dissolved in DMSO 3 h prior to 1st or 2nd rounds of 2-AA exposure.
530 RAW264.7 macrophages supplemented with ATP (20 μM, Sigma-Aldrich, dissolved in PBS)
531 received ATP at the time of 1st and 2nd 2-AA exposure.

532 **Co-Immunoprecipitation assay**

533 For all immunoprecipitation assays, protein A/G agarose Magnetic beads (Pierce) were used
534 after washing in 1X IP buffer. Nuclear lysates from RAW 264.7 tolerized cells exposed to 2-AA
535 for 24 h or non-exposed cells were diluted in 1X IP buffer and 500 μg of protein was taken for
536 each experiment. The lysates were precleared by using unbound 50 μl protein A/G magnetic
537 beads for 2 h at room temperature on a rotator. Precleared lysates were either incubated with
538 ERRα, PGC-1α or rabbit IgG antibody overnight at 4 °C. 100 μl protein A/G magnetic beads
539 were used to pull down the antibody-protein complex and washed twice with IP buffer to
540 remove unbound proteins. Magnetic beads were then eluted in 2X Laemmli SDS-PAGE
541 loading buffer. Immunoprecipitated ERRα and PGC-1α was detected by Western blot
542 analyses, using conformational specific Anti Rabbit antibody (TruBlot).

543 **Immunoblotting analysis**

544 Cells were plated at 6×10^5 cells per well in six-well plates. Cells were washed with PBS and
545 subsequently lysed using RIPA lysis buffer containing 1 mM phenylmethylsulfonyl fluoride
546 (PMSF). 20μg of proteins were separated by electrophoresis on any KD (Kilo Dalton) (Bio-
547 Rad, Cat no. 4569033) SDS-polyacrylamide gel. Proteins were transferred to a 0.2 μm
548 polyvinylidene fluoride membrane (PVDF, Millipore, Billerica, USA) using a Bio-Rad semi-dry
549 instrument. After blocking with 5% BSA in TBS containing 0.1% Tween-20 for 1 h at room
550 temperature, the membranes were incubated with a primary antibody ERR-a (Abcam,
551 #ab76228), MPC1 (D2L91, Cell signaling), and anti-β-actin (cat no: sc-47778) (Santa Cruz
552 Biotechnology) overnight at 4°C. Following washing, the membranes were incubated with an

553 anti-rabbit secondary antibody, and the bands were detected by SuperSignal West Pico
554 Chemiluminescent Substrate (Thermo Scientific) reaction, according to the manufacturer's
555 instructions. The blots were visualized in the ChemiDOC Imaging system (Bio-Rad
556 Laboratories, Inc., Hercules, CA, USA). The bands were analyzed densitometrically using
557 QuantityOne software (Bio-Rad).

558 **Chromatin immunoprecipitation (ChIP) and ChIP-qPCR**

559 For ChIP studies, RAW264.7 macrophage cells exposed to 2-AA for 24 h were cross-linked in
560 1% (v/v) methanol-free formaldehyde for 10 min and then placed in 0.125 M glycine for 5 min
561 at RT. Using the truChIP High Cell Chromatin Shearing kit (Covaris, United States), cells were
562 prepared for sonication according to the Covaris protocol. Approximately 1×10^7 cells were
563 plated in a 12 mm × 12 mm tube and subjected to shearing with the Covaris S220 sonicator for
564 8 min (140 peak power, 5 duty factor, 200 cycles/burst). The Magna ChIP A/G kit (Millipore,
565 United States) was used for the subsequent immunoprecipitations according to the
566 manufacturer's protocol. Briefly, chromatin from approximately 10^6 cells was incubated
567 overnight at 4°C with 2 μg of anti-ERRα or anti-PGC-1α (Abcam, USA) ChIP-grade antibody
568 and 20 μL of A/G magnetic beads. The beads were washed serially (5 min each) with low-salt
569 wash buffer, high-salt wash buffer, LiCl wash buffer, and TE buffer from the kit at 4°C.
570 Chromatin was eluted with elution buffer containing Proteinase K at 62°C for 4 h, then
571 incubated at 95°C for 10 min. DNA was isolated by column purification (QIAquick PCR
572 purification kit).

573 Real-time ChIP-qPCR was performed with the Brilliant II SYBR green super mix (Agilent, USA).
574 Forward (AGTGGTGACCTTGAACTTCCC) and reverse (CTGAAGACGACCTTCCCCTT)
575 primers were chosen to amplify a genomic locus of *MPC1* promoter which had a putative ERR
576 binding site (gtgaccttg) at 1582 bp upstream of the start site. Normalized values were
577 calculated by the percent-input method relative to the IgG. The assay was performed three
578 times.

579 **RNA extraction and RT-qPCR**

580 Total RNA from all the groups mentioned above was isolated from approximately 2 × 10^6 cells
581 with the RNeasy minikit (Qiagen, USA), and cDNA was prepared with the iScript Reverse
582 transcription kit (Bio-Rad, USA), as per the manufacturer's instruction. Real-time PCR was
583 conducted using the PowerUP SYBR green Master mix (Applied Biosystem, USA) and primer
584 sets for mouse ERR-α (forward: ACTACGGTGTGGCATCCTGTGA; reverse:
585 GGTGATCTCACACTCATTGGAGG), MPC-1 (forward: CTCCAGAGATTATCAGTGGGCG;
586 reverse: GAGCTACTTCGTTTGTTACATGGC), TNF-α (forward:
587 GGTGCCTATGTCTCAGCCTCTT; reverse: GCCATAGAACTGATGAGAGGGAG) and mouse
588 18S rRNA (forward: GTTCCGACCATAAACGATGCC; reverse:
589 TGGTGGTGCCCTTCCGTCAAT). The transcript levels of all the genes were normalized to
590 18S rRNA with the ΔΔCT method. The relative expression was calculated by normalizing
591 transcript levels to those of PA14 Infected cells. The assay was conducted in triplicate; means
592 and standard deviations were calculated for each group.

593 **Animal infection and metabolites assessment experiments**

594 The full-thickness thermal burn injury and infection (BI) model [17, 18, 72] was used to assess
595 the effect of 2-AA on metabolic alterations in the spleens of six-week-old CD1 male mice and
596 bacterial burden (Charles River Labs, USA). A full-thickness thermal burn injury involving 5-
597 8% of the total body surface area was produced on the shaved mouse abdomen dermis, and
598 an inoculum of ~1 × 10^4 PA14 and Δ*mvfR* [19] cells in 100 μL of $MgSO_4$ (10 mM) was injected
599 intradermally into the burn eschar. For the groups that received 2-AA, mice were injected
600 intraperitoneally (IP) with 100 μL of 2-AA (6.75 mg/kg). The entire procedure was done under
601 the influence of anesthesia. One of the groups of mice infected with the PA14 isogenic mutant
602 Δ*mvfR* [19] also received 100 μL of 2-AA in PBS (6.75 mg/kg) at the time of infection (Δ*mvfR*
603 +2-AA) and served as an additional control. CFU counts from rectus abdominus muscle
604 (underlying the burn-infected tissue) were assessed in groups of 4 mice each at 1, 5, and 10

605 d post-BI by plating diluted muscle homogenate on Pseudomonas isolation agar (Sigma-
606 Aldrich) plates containing rifampicin (50 mg/L). Spleen samples from mice were collected for
607 metabolite analyses from all mice groups at 1, 5, and 10 d post-BI to assess ATP (#ab83355
608 Abcam) and acetyl-CoA (#ab87546, Abcam) as described above. Tissues were homogenized,
609 and 100 mg of homogenate was centrifuged at 4°C for 15 min at 10,000 g, and supernatants
610 were collected. The supernatant was mixed with 400 µL of 1 M perchloric acid. The
611 deproteinized supernatant was neutralized by 3 M $KHCO_3$. The ATP and acetyl-CoA assays
612 were performed as described in the *in vitro* section.

613 **Acknowledgments and Funding sources**

614 We thank Dr. Vamsi Mootha and Sneha Rath for access and help with the Seahorse
615 instrument, respectively. This work was supported by the NIH award R01AI134857, The John
616 Lawrence Massachusetts General Hospital Research Scholar Award and Shriner's grant
617 83009 to L.G.R., and the Shriner's grant 85132 to A.A.T. The funders had no role in the study
618 design, data collection, analysis, decision to publish, or manuscript preparation.

619

620 **Figures**

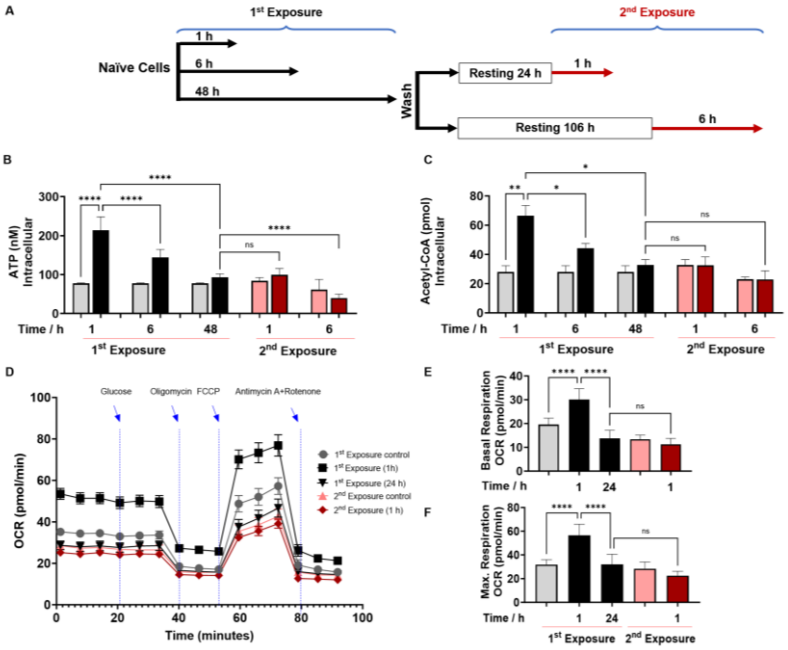

621

622 **Figure 1**

623

624

625

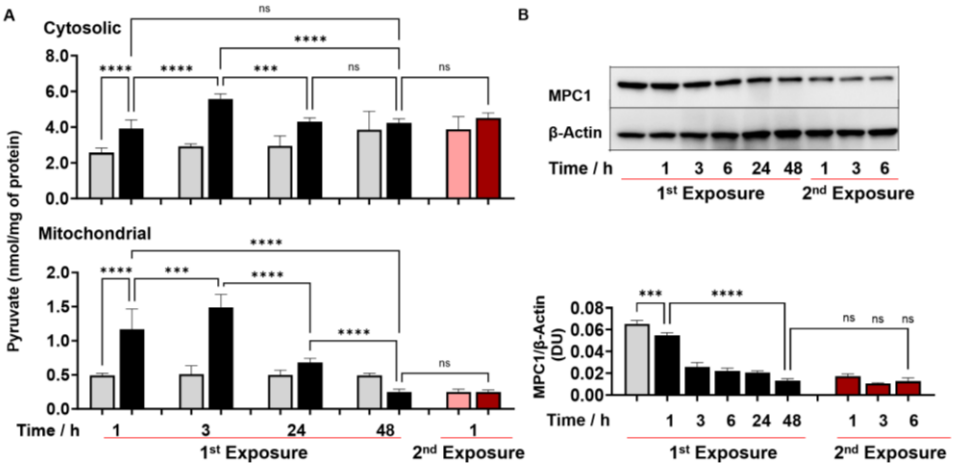

Figure 2

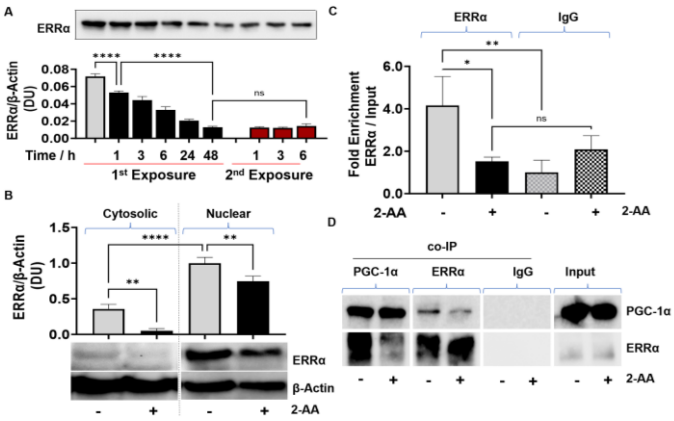

Figure 3

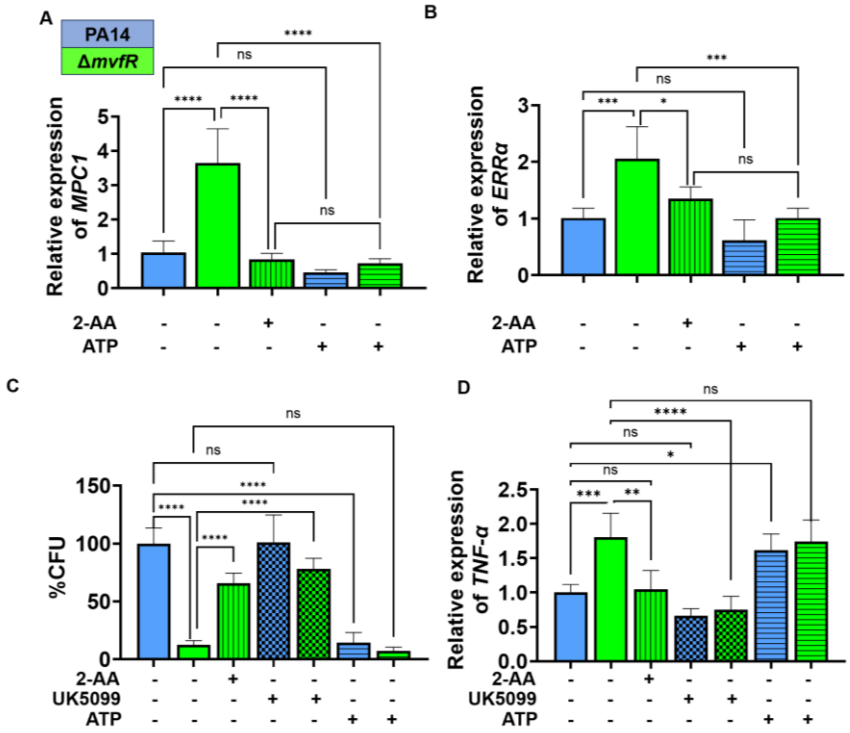
A
PA14
ΔmvfR
Relative expression of MPC1
2-AA
ATP
B
Relative expression of ERRα
2-AA
ATP
C
%CFU
2-AA
UK5099
ATP
D
Relative expression of TNF-α
2-AA
UK5099
ATP

Figure 4

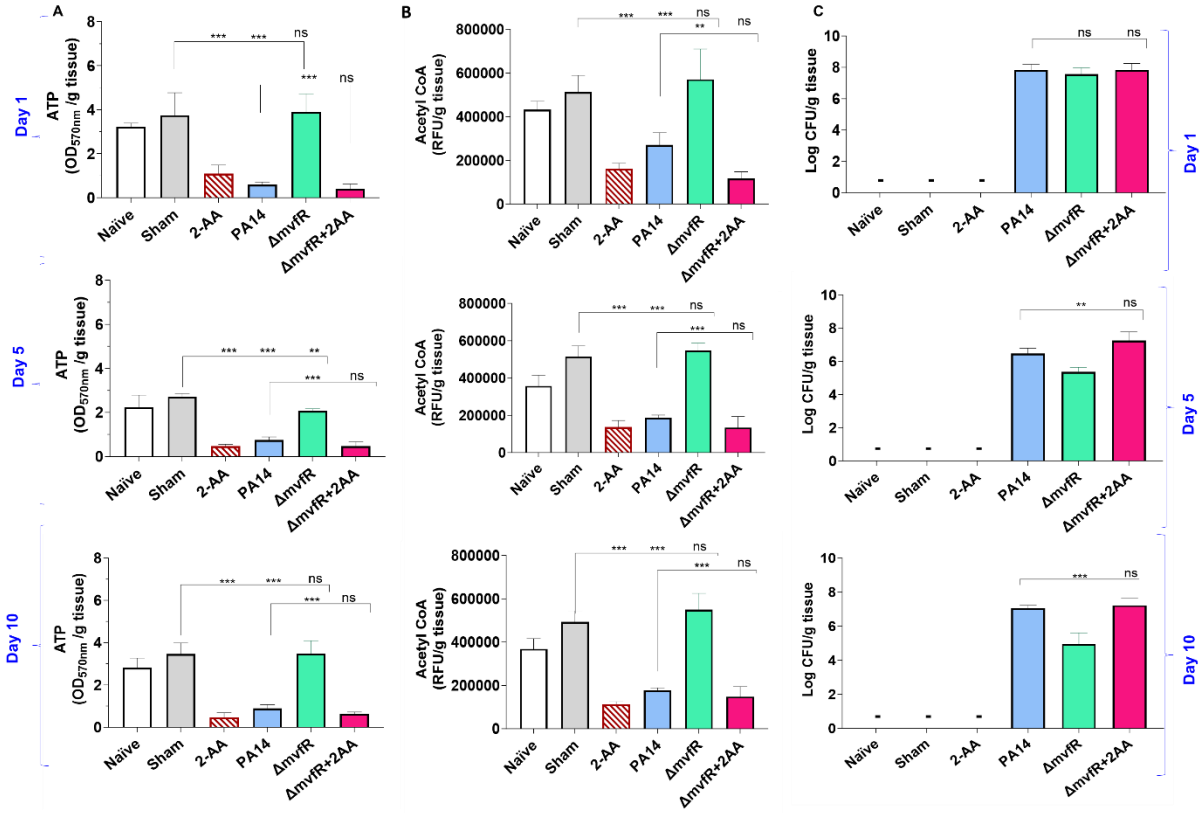

635

636 **Figure 5**

637

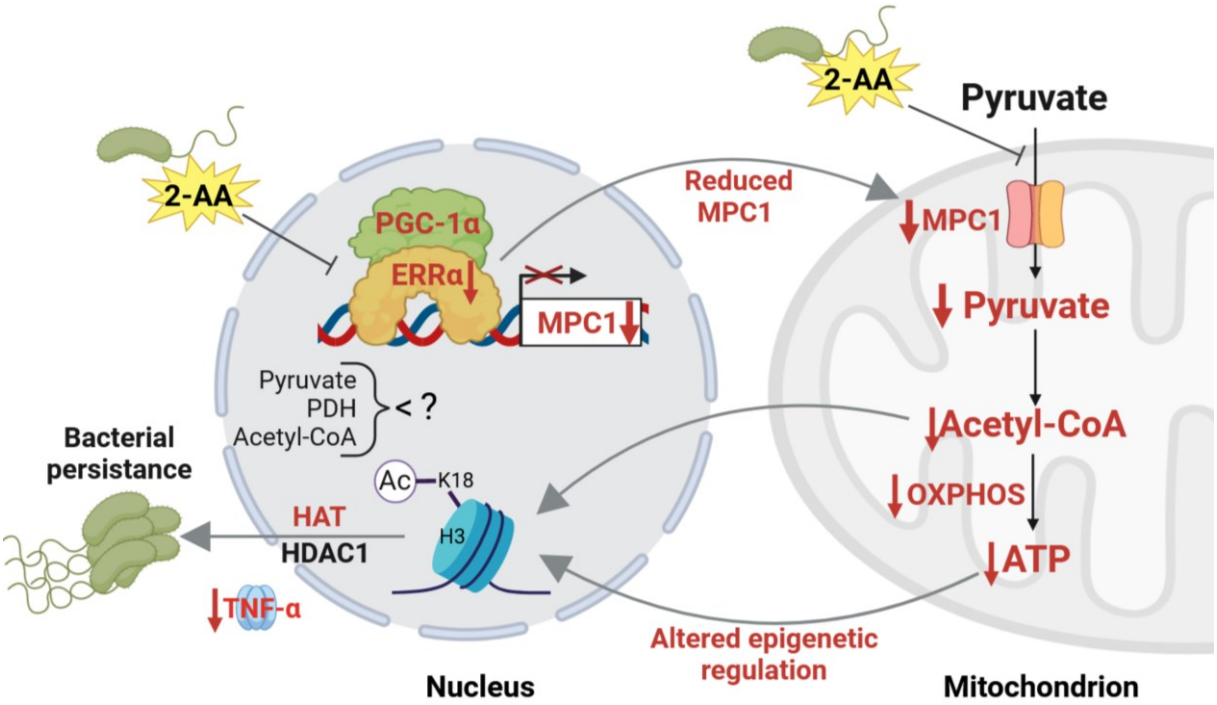
2-AA
2-AA
Pyruvate
Reduced
MPC1
PGC-1α
ERRα
MPC1
MPC1
Pyruvate
Pyruvate
PDH
Acetyl-CoA
< ?
Acetyl-CoA
Bacterial
persistance
Ac
K18
H3
HAT
HDAC1
OXPHOS
ATP
TNF-α
Altered epigenetic
regulation
Nucleus
Mitochondrion

Figure 6

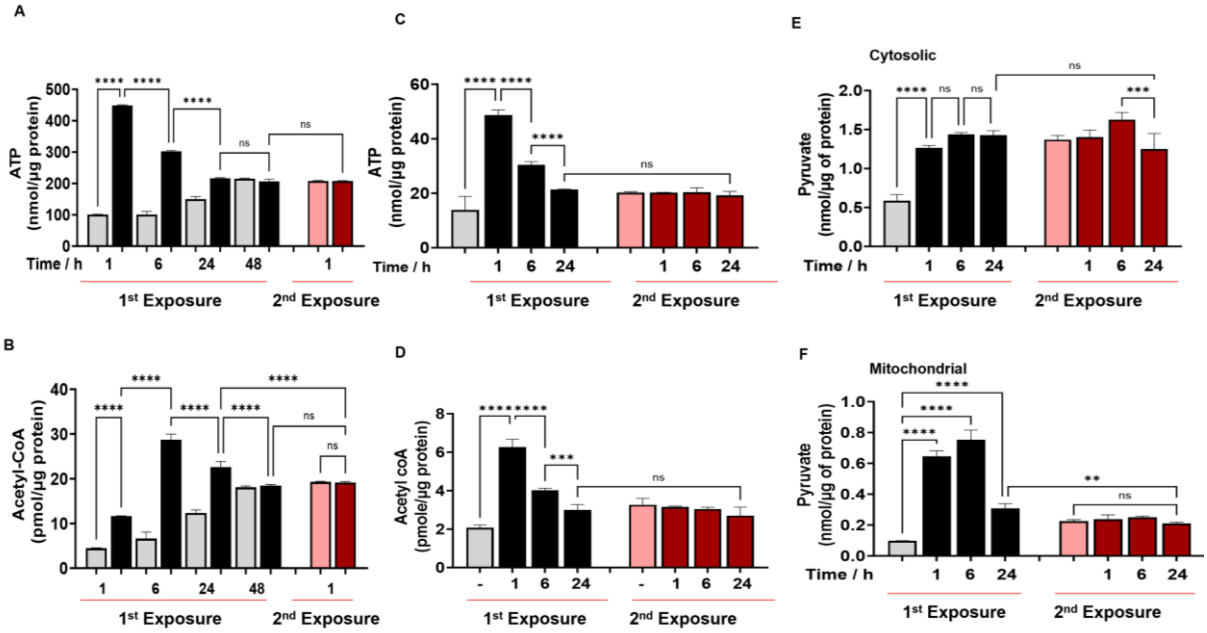

642

643 **Figure S1**

644

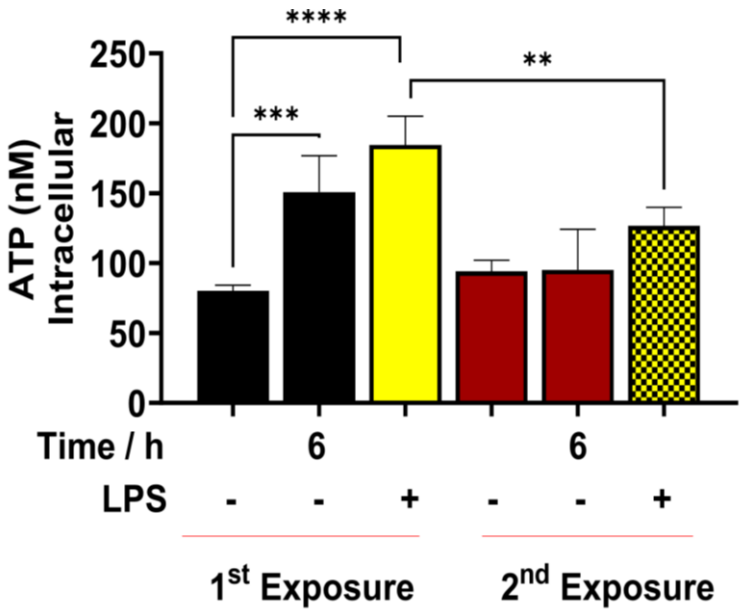

645

646 **Figure S2**

647

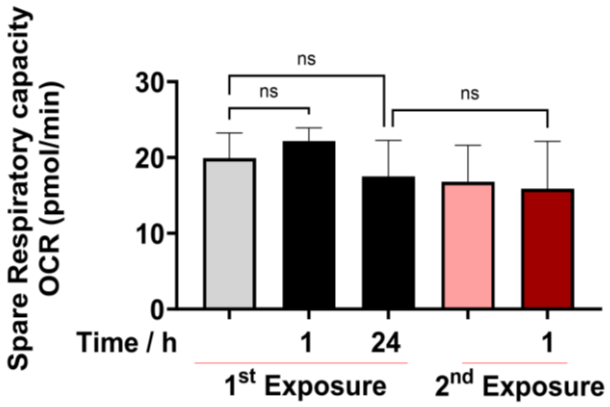

648

649 **Figure S3**

650

651

652 **Figure Legends**

653 **Figure 1. 2-AA tolerization decreases crucial metabolites of cellular energy and affects**
654 **mitochondrial respiration in mouse BMDM.** (A) Schematic representation showing
655 experimental design: naïve cells were exposed to 2-AA for 1, 6, or 48 h (black). Cells exposed
656 to 2-AA (400 μM) for 48 h were washed, rested for 24 or 106 h, and re-exposed (200 μM) for
657 1 or 6 h (red), respectively. The same color code: black: cells after 1st exposure; red: cells after
658 2ndexposure, was kept throughout the manuscript with corresponding controls in grey and pink,
659 respectively. The levels of (B) ATP and (C) acetyl-CoA in BMDM cells after 1st and 2nd 2-AA
660 exposure. (D) Real-time oxygen consumption rate (OCR) traces were recorded using a
661 Seahorse XF analyzer and normalized to protein content. Cells were exposed to 2-AA for 1 or
662 24 h (black), washed and rested for 24 h and re-exposed for 1 h (red). Mitochondrial respiratory
663 parameters, (E) basal respiration, and (F) maximal respiration. Data are presented as
664 mean ± SD. n ≥ 4, *p < 0.05, **p < 0.01, ***p < 0.001, and ns indicates no significant difference.
665 One-way ANOVA followed by Tukey's post hoc test was applied.

666 **Figure 2. 2-AA perturbs the mitochondrial MPC1-mediated import and metabolism of**
667 **pyruvate.** (A) Cytosolic and mitochondrial pyruvate levels following 2-AA exposure (black) or
668 re-exposure (red) and corresponding controls in grey and pink respectively, for indicated time
669 points. (B) Representative Western blot and results of densitometric analysis of MPC1 protein
670 levels following 2-AA exposure or re-exposure for indicated time points. β-actin was used as a
671 control. Corresponding controls are shown in grey or pink, respectively. Mean ± SD is shown;
672 n = 3; ***p < 0.001, ****p < 0.0001, and ns indicates no significant difference. One-way ANOVA
673 followed by Tukey's post hoc test was applied.

674 **Figure 3: 2-AA-mediated macrophage tolerization deranges PGC-1α/ERRα-dependent**
675 **metabolic programing.** (A) Representative Western blot and results of densitometric analysis
676 of ERRα protein levels following 2-AA exposure or re-exposure for indicated time points. β-

677 actin (Fig. 2B) was used as a control. (B) Western blots and its corresponding densitometric
678 analysis of ERRα in cytoplasmic or nuclear lysates of tolerized macrophages exposed to 2-AA
679 for 24 h or not exposed to 2-AA. (C) ChIP-qPCR assay of ERRα binding at the MPC1 promoter
680 in RAW 264.7 tolerized macrophages exposed to 2-AA (200 μM) for 24 h (black) compared to
681 untreated control macrophages (grey). IgG served as a negative control (D) Representative
682 Western blot of co-immunoprecipitation (co-IP) studies of ERRα and PGC-1α in nuclear
683 extracts of 2-AA tolerized (24 h) and control RAW 264.7 cells. Pull down with IgG served as a
684 negative control. 2-AA tolerized macrophages are shown in black, and untreated control
685 macrophages in grey. Mean ± SD in shown, n ≥ 3, *$p < 0.05$, **$p < 0.01$, ****$p < 0.0001$, and
686 ns indicates no significant difference. One-way ANOVA followed by Tukey's post hoc test was
687 applied.

688 **Figure 4: Increased intracellular burden in macrophages is associated with decreased**
689 **expression of *MPC1, ERR-α,* and *TNF-α genes*.** Real-time PCR analysis of *MPC1* (A) and
690 *ERR-α* (B) expression in RAW 246.7 macrophages infected with PA14 or *ΔmvfR* in the
691 presence or absence of exogenous addition of 2-AA or ATP for 6 h as indicated. Transcript
692 levels were normalized to 18srRNA. PA14 infected cells served as controls. (C) Intracellular
693 burden of PA14 or Δ*mvfR* of infected macrophages in the presence or absence of exogenous
694 addition of 2-AA, UK5099, or ATP. Untreated cells infected with PA14 were set as 100%. D)
695 Real-time PCR analysis of TNF-α expression in RAW 246.7 macrophages infected with PA14
696 or Δ*mvfR* in the presence or absence of exogenous addition of 2-AA, ATP, or UK5099.
697 Transcript levels were normalized to 18srRNA. PA14 infected cells served as controls. The
698 compound concentration used for UK5099 was 10 μM and ATP 20 μM. Mean ± SD is shown
699 ($n = 3$); * $p < 0.05$, **$p < 0.01$, ***$p < 0.001$, ****$p < 0.0001$***, and ns indicates no significant
700 difference. One-way ANOVA followed by Tukey's post hoc test was applied.

701 **Figure 5. 2-AA promotes a long-lasting decrease in ATP and acetyl-CoA levels and**
702 **bacterial persistence in *PA*-infected mice.** (A) ATP and (B) acetyl-CoA concentrations in the
703 spleens of mice infected with *PA* wild type (PA14), the isogenic mutant Δ*mvfR*, Δ*mvfR* injected
704 with 2-AA at the time of infection (Δ*mvfR* + 2-AA), or non-infected but injected with 2-AA (6.75
705 mg/kg). (C) Bacterial burden in muscles expressed as CFU count was analyzed using the
706 Kruskal–Wallis non-parametric test with Dunn's post-test; ***$p < 0.001$, and ns indicates no
707 significant difference. Control mice groups: naïve were not given 2-AA; mice receiving 2-AA
708 were given a single intraperitoneal injection of 2-AA; sham represents a burn/PBS group since
709 the burn and infection model was used. Results of three independent replicates with 4 mice
710 per group for 1, 5, and 10 d are shown. Means ± SD are shown: *$p < 0.05$, **$p < 0.01$, ***$p <$
711 0.001, and ns indicate no significant difference. One-way ANOVA followed by Tukey's post hoc
712 test was applied.

713

714 **Figure 6: Proposed mechanism by which 2-AA impairs bioenergetics through the**
715 **inhibition of MPC1-mediated pyruvate transport into mitochondria and its impact on the**
716 **PGC-1α/ERRα axis.** 2-AA tolerized macrophages exhibit diminished pyruvate levels in
717 mitochondria due to the decreased expression of *MPC1*, a consequence of the 2-AA impact
718 on the interaction of ERRα with the transcriptional coactivator PGC-1α for the effective
719 transcription of ERRα, since ERRα controls its own transcription and that of MPC1. In the
720 presence of 2-AA, the weakened interaction between ERRα and PGC-1α results in reduced
721 expression of MPC1 and ERRα. The reduction in mitochondrial pyruvate levels leads to
722 decreased acetyl-CoA and ATP levels, which modulate HDAC1- and HAT-catalyzed
723 remodeling of H3K18 acetylation. The diminished levels of this epigenetic mark have
724 previously been associated with an increased intracellular presence of bacteria in
725 macrophages, as demonstrated by our group [18]. Pathways, proteins, and metabolites that

726 are negatively affected are indicated in red, while positively affected are denoted in black. The
727 figure was created using BioRender.com.

728 **Figure S1.** 2-AA tolerization decreases metabolites in murine RAW 264.7 (A-B) and human
729 THP-1 (C-D) cells. (A and C) ATP, (B and D) acetyl-CoA and (E) cytosolic and (F) mitochondrial
730 pyruvate levels were quantified in 2-AA (400 μM) exposed and re-exposed cells for the hours
731 indicated using the same condition as shown in Fig. 1A. Mean ± SD is shown (n = 3); *** p <
732 0.001, and ns indicates no significant difference. One-way ANOVA followed by Tukey's post
733 hoc test was applied. The same color code: black, cells after 1st exposure; red, cells after 2nd
734 exposure was kept as throughout the main manuscript with corresponding controls shown in
735 grey and pink, respectively.

736 **Figure S2:** ATP levels in murine BMDM (A) cells with and without 2-AA (400 μM) or LPS
737 stimulation (100 μg/mL). Each dot represents 1 experimental replicate of 4 independent
738 experiments (n = 4). Data are presented as mean ± SD. **p < 0.01, ***p < 0.001, and ns
739 indicates no significant difference. One-way ANOVA followed by Tukey's post hoc test was
740 applied.

741 **Figure S3**: Effect of 2-AA on mitochondrial spare respiratory capacity in BMDM non-tolerized
742 (black) and tolerized (red) macrophages. Controls are shown in grey and pink, respectively.
743 Mitochondrial spare respiratory capacity data extrapolated from the OCR profiles shown in
744 Figure 1D. Unstimulated BMDM macrophages were used as a control (c). Means ± SDs are
745 shown (n = 6); * p < 0.05, *** p < 0.001, and ns indicates no significant difference. One-way
746 ANOVA followed by Tukey's post hoc test was applied.

747

748

749

References

1. Foster, S.L., D.C. Hargreaves, and R. Medzhitov, *Gene-specific control of inflammation by tlr-induced chromatin modifications.* Nature, 2007. **447**(7147): p. 972.
2. Bagchi, A., et al., *Myd88-dependent and myd88-independent pathways in synergy, priming, and tolerance between tlr agonists.* Journal of immunology, 2007. **178**(2): p. 1164.
3. Masyutina, A.M., et al., *Inhibition of specific signaling pathways rather than epigenetic silencing of effector genes is the leading mechanism of innate tolerance.* Frontiers in Immunology, 2023. **14**.
4. O'Neill, L.A., R.J. Kishton, and J. Rathmell, *A guide to immunometabolism for immunologists.* Nat Rev Immunol, 2016. **16**(9): p. 553.
5. Chi, H., *Immunometabolism at the intersection of metabolic signaling, cell fate, and systems immunology.* Cellular & Molecular Immunology, 2022. **19**(3): p. 299.
6. Tannahill, G.M., et al., *Succinate is an inflammatory signal that induces il-1beta through hif-1alpha.* Nature, 2013. **496**(7444): p. 238.
7. Galli, G. and M. Saleh, *Immunometabolism of macrophages in bacterial infections.* Front Cell Infect Microbiol, 2020. **10**: p. 607650.
8. Wang, Y., et al., *Mitochondrial metabolism regulates macrophage biology.* J Biol Chem, 2021. **297**(1): p. 100904.
9. Karan, K.R., et al., *Leukocyte cytokine responses in adult patients with mitochondrial DNA defects.* Journal of Molecular Medicine, 2022. **100**(6): p. 963.
10. Bird, L., *Getting enough energy for immunity.* Nature Reviews Immunology, 2019. **19**(5): p. 269.
11. Deziel, E., et al., *The contribution of mvfr to pseudomonas aeruginosa pathogenesis and quorum sensing circuitry regulation: Multiple quorum sensing-regulated genes are modulated without affecting lasri, rhlri or the production of n-acyl-l-homoserine lactones.* Mol Microbiol, 2005. **55**(4): p. 998.
12. Xiao, G., et al., *Mvfr, a key pseudomonas aeruginosa pathogenicity lttr-class regulatory protein, has dual ligands.* Mol Microbiol, 2006. **62**(6): p. 1689.
13. Eickhoff, M.J. and B.L. Bassler, *Snapshot: Bacterial quorum sensing.* Cell, 2018. **174**(5): p. 1328.
14. Fuqua, C. and E.P. Greenberg, *Listening in on bacteria: Acyl-homoserine lactone signalling.* Nature Reviews Molecular Cell Biology, 2002. **3**(9): p. 685.
15. Kariminik, A., M. Baseri-Salehi, and B. Kheirkhah, *Pseudomonas aeruginosa quorum sensing modulates immune responses: An updated review article.* Immunol Lett, 2017. **190**: p. 1.
16. Liu, Y.C., K.G. Chan, and C.Y. Chang, *Modulation of host biology by pseudomonas aeruginosa quorum sensing signal molecules: Messengers or traitors.* Front Microbiol, 2015. **6**: p. 1226.
17. Bandyopadhaya, A., et al., *The quorum sensing volatile molecule 2-amino acetophenon modulates host immune responses in a manner that promotes life with unwanted guests.* PLoS pathogens, 2012. **8**(11): p. e1003024.
18. Bandyopadhaya, A., et al., *A quorum-sensing signal promotes host tolerance training through hdac1-mediated epigenetic reprogramming.* Nat Microbiol, 2016. **1**: p. 16174.
19. Cao, H., et al., *A quorum sensing-associated virulence gene of pseudomonas aeruginosa encodes a lysr-like transcription regulator with a unique self-regulatory mechanism.* Proceedings of the National Academy of Sciences of the United States of America, 2001. **98**(25): p. 14613.
20. Deziel, E., et al., *Analysis of pseudomonas aeruginosa 4-hydroxy-2-alkylquinolines (haqs) reveals a role for 4-hydroxy-2-heptylquinoline in cell-to-cell communication.* Proc Natl Acad Sci U S A, 2004. **101**(5): p. 1339.

21. Kesarwani, M., et al., *A quorum sensing regulated small volatile molecule reduces acute virulence and promotes chronic infection phenotypes.* PLoS Pathog, 2011. **7**(8): p. e1002192.
22. Bandyopadhaya, A., A. Tsurumi, and L.G. Rahme, *Nf-kappabp50 and hdac1 interaction is implicated in the host tolerance to infection mediated by the bacterial quorum sensing signal 2-aminoacetophenone.* Front Microbiol, 2017. **8**: p. 1211.
23. Wheeler, D.S., et al., *Induction of endotoxin tolerance enhances bacterial clearance and survival in murine polymicrobial sepsis.* Shock, 2008. **30**(3): p. 267.
24. Tzika, A.A., et al., *A small volatile bacterial molecule triggers mitochondrial dysfunction in murine skeletal muscle.* Plos One, 2013. **8**(9): p. e74528.
25. Bandyopadhaya, A., et al., *Bacterial-excreted small volatile molecule 2-aminoacetophenone induces oxidative stress and apoptosis in murine skeletal muscle.* International Journal of Molecular Medicine, 2016. **37**(4): p. 867.
26. Chakraborty, A., et al., *Quorum-sensing signaling molecule 2-aminoacetophenone mediates the persistence of pseudomonas aeruginosa in macrophages by interference with autophagy through epigenetic regulation of lipid biosynthesis.* mBIo, 2023: p. e0015923.
27. Maurice, N.M., et al., *Pseudomonas aeruginosa induced host epithelial cell mitochondrial dysfunction.* Scientific Reports, 2019. **9**(1).
28. Lelliott, C.J. and A. Vidal-Puig, *Pgc-1beta: A co-activator that sets the tone for both basal and stress-stimulated mitochondrial activity.* Adv Exp Med Biol, 2009. **646**: p. 133.
29. Supruniuk, E., A. Mikłosz, and A. Chabowski, *The implication of pgc-1α on fatty acid transport across plasma and mitochondrial membranes in the insulin sensitive tissues.* Front Physiol, 2017. **8**: p. 923.
30. Coppi, L., et al., *Pgc1s and beyond: Disentangling the complex regulation of mitochondrial and cellular metabolism.* International Journal of Molecular Sciences, 2021. **22**: p. 6913.
31. Lin, J., C. Handschin, and B.M. Spiegelman, *Metabolic control through the pgc-1 family of transcription coactivators.* Cell Metab, 2005. **1**(6): p. 361.
32. Huss, J.M., W.G. Garbacz, and W. Xie, *Constitutive activities of estrogen-related receptors: Transcriptional regulation of metabolism by the err pathways in health and disease.* Biochim Biophys Acta, 2015. **1852**(9): p. 1912.
33. Schreiber, S.N., et al., *The transcriptional coactivator pgc-1 regulates the expression and activity of the orphan nuclear receptor estrogen-related receptor alpha (erralpha).* J Biol Chem, 2003. **278**(11): p. 9013.
34. Laganière, J., et al., *A polymorphic autoregulatory hormone response element in the human estrogen-related receptor α (errα) promoter dictates peroxisome proliferator-activated receptor γ coactivator-1α control of errα expression*.* Journal of Biological Chemistry, 2004. **279**(18): p. 18504.
35. Villena, J.A., *New insights into pgc-1 coactivators: Redefining their role in the regulation of mitochondrial function and beyond.* The FEBS journal, 2015. **282**(4): p. 647.
36. Ranhotra, H.S., *The estrogen-related receptor alpha: The oldest, yet an energetic orphan with robust biological functions.* J Recept Signal Transduct Res, 2010. **30**(4): p. 193.
37. Deblois, G. and V. Giguère, *Functional and physiological genomics of estrogen-related receptors (errs) in health and disease.* Biochim Biophys Acta, 2011. **1812**(8): p. 1032.
38. Ranhotra, H.S., *The estrogen-related receptors: Orphans orchestrating myriad functions.* J Recept Signal Transduct Res, 2012. **32**(2): p. 47.
39. Charest-Marcotte, A., et al., *The homeobox protein prox1 is a negative modulator of err{alpha}/pgc-1{alpha} bioenergetic functions.* Genes Dev, 2010. **24**(6): p. 537.
40. Eichner, L.J. and V. Giguère, *Estrogen related receptors (errs): A new dawn in transcriptional control of mitochondrial gene networks.* Mitochondrion, 2011. **11**(4): p. 544.
41. Koh, E., et al., *Mpc1 is essential for pgc-1α-induced mitochondrial respiration and biogenesis.* Biochem J, 2018. **475**(10): p. 1687.

42. Divangahi, M., et al., *Trained immunity, tolerance, priming and differentiation: Distinct immunological processes.* Nat Immunol, 2021. **22**(1): p. 2.
43. Xue, C., et al., *Mitochondrial pyruvate carrier 1: A novel prognostic biomarker that predicts favourable patient survival in cancer.* Cancer Cell Int, 2021. **21**(1): p. 288.
44. Bronte, V. and M.J. Pittet, *The spleen in local and systemic regulation of immunity.* Immunity, 2013. **39**(5): p. 806.
45. Starkey, M., et al., *Identification of anti-virulence compounds that disrupt quorum-sensing regulated acute and persistent pathogenicity.* PLoS pathogens, 2014. **10**(8): p. e1004321.
46. Dulcey, C.E., et al., *The end of an old hypothesis: The pseudomonas signaling molecules 4-hydroxy-2-alkylquinolines derive from fatty acids, not 3-ketofatty acids.* Chem Biol, 2013. **20**(12): p. 1481.
47. Fetzner, S. and S.L. Drees, *Old molecules, new biochemistry.* Chem Biol, 2013. **20**(12): p. 1438.
48. Park, S., et al., *Inhibition of erralpha prevents mitochondrial pyruvate uptake exposing nadph-generating pathways as targetable vulnerabilities in breast cancer.* Cell Rep, 2019. **27**(12): p. 3587.
49. Caslin, H.L., et al., *Lactate is a metabolic mediator that shapes immune cell fate and function.* Front Physiol, 2021. **12**: p. 688485.
50. Lee, T.Y., *Lactate: A multifunctional signaling molecule.* Yeungnam Univ J Med, 2021. **38**(3): p. 183.
51. Li, X., et al., *Lactate metabolism in human health and disease.* Signal Transduction and Targeted Therapy, 2022. **7**(1): p. 305.
52. Wei, W., et al., *Ligand activation of errα by cholesterol mediates statin and bisphosphonate effects.* Cell metabolism, 2016. **23**(3): p. 479.
53. Chisamore, M.J., et al., *Identification of small molecule estrogen-related receptor α–specific antagonists and homology modeling to predict the molecular determinants as the basis for selectivity over errβ and errγ.* Drug development research, 2008. **69**(4): p. 203.
54. Mayer, M.L., et al., *The pseudomonas aeruginosa autoinducer 3o-c12 homoserine lactone provokes hyperinflammatory responses from cystic fibrosis airway epithelial cells.* PloS one, 2011. **6**(1): p. e16246.
55. Kushwaha, A., V. Kumar, and V. Agarwal, *Pseudomonas quinolone signal induces organelle stress and dysregulates inflammation in human macrophages.* Biochim Biophys Acta Gen Subj, 2023. **1867**(2): p. 130269.
56. Pietrocola, F., et al., *Acetyl coenzyme a: A central metabolite and second messenger.* Cell Metab, 2015. **21**(6): p. 805.
57. Chandran, A., et al., *Mycobacterium tuberculosis infection induces hdac1-mediated suppression of il-12b gene expression in macrophages.* Front Cell Infect Microbiol, 2015. **5**: p. 90.
58. Shi, L. and B.P. Tu, *Acetyl-coa and the regulation of metabolism: Mechanisms and consequences.* Curr Opin Cell Biol, 2015. **33**: p. 125.
59. Lauterbach, M.A., et al., *Toll-like receptor signaling rewires macrophage metabolism and promotes histone acetylation via atp-citrate lyase.* Immunity, 2019. **51**(6): p. 997.
60. Saeed, S., et al., *Epigenetic programming of monocyte-to-macrophage differentiation and trained innate immunity.* Science, 2014. **345**(6204): p. 1251086.
61. Liu, T.F., et al., *Nad+-dependent sirtuin 1 and 6 proteins coordinate a switch from glucose to fatty acid oxidation during the acute inflammatory response.* J Biol Chem, 2012. **287**(31): p. 25758.
62. Ishida, K., et al., *Chlamydia pneumoniae effector chlamydial outer protein n sequesters fructose bisphosphate aldolase a, providing a benefit to bacterial growth.* BMC Microbiol, 2014. **14**: p. 330.

63. Kunze, M., et al., *Metabolic adaption of legionella pneumophila during intracellular growth in acanthamoeba castellanii.* Int J Med Microbiol, 2021. **311**(4): p. 151504.
64. Shi, L., et al., *Infection with mycobacterium tuberculosis induces the warburg effect in mouse lungs.* Sci Rep, 2015. **5**: p. 18176.
65. Perez-Morales, D. and V.H. Bustamante, *Cross-kingdom metabolic manipulation promotes salmonella replication inside macrophages.* Nat Commun, 2021. **12**(1): p. 1862.
66. Dhamgaye, S., Y. Qu, and A.Y. Peleg, *Polymicrobial infections involving clinically relevant gram-negative bacteria and fungi.* Cellular microbiology, 2016. **18**(12): p. 1716.
67. Vega, R.B., J.M. Huss, and D.P. Kelly, *The coactivator pgc-1 cooperates with peroxisome proliferator-activated receptor alpha in transcriptional control of nuclear genes encoding mitochondrial fatty acid oxidation enzymes.* Molecular and cellular biology, 2000. **20**(5): p. 1868.
68. Bekkering, S., et al., *Trained immunity: Reprogramming innate immunity in health and disease.* Annual Review of Immunology, 2021. **39**(1): p. 667.
69. Ochando, J., et al., *Trained immunity — basic concepts and contributions to immunopathology.* Nature Reviews Nephrology, 2023. **19**(1): p. 23.
70. Au - Van den Bossche, J., J. Au - Baardman, and M.P.J. Au - de Winther, *Metabolic characterization of polarized m1 and m2 bone marrow-derived macrophages using real-time extracellular flux analysis.* JoVE, 2015(105): p. e53424.
71. Rahme, L.G., et al., *Common virulence factors for bacterial pathogenicity in plants and animals.* Science, 1995. **268**(5219): p. 1899.
72. Maura, D., A. Bandyopadhaya, and L.G. Rahme, *Animal models for pseudomonas aeruginosa quorum sensing studies.* Methods Mol Biol, 2018. **1673**: p. 227.

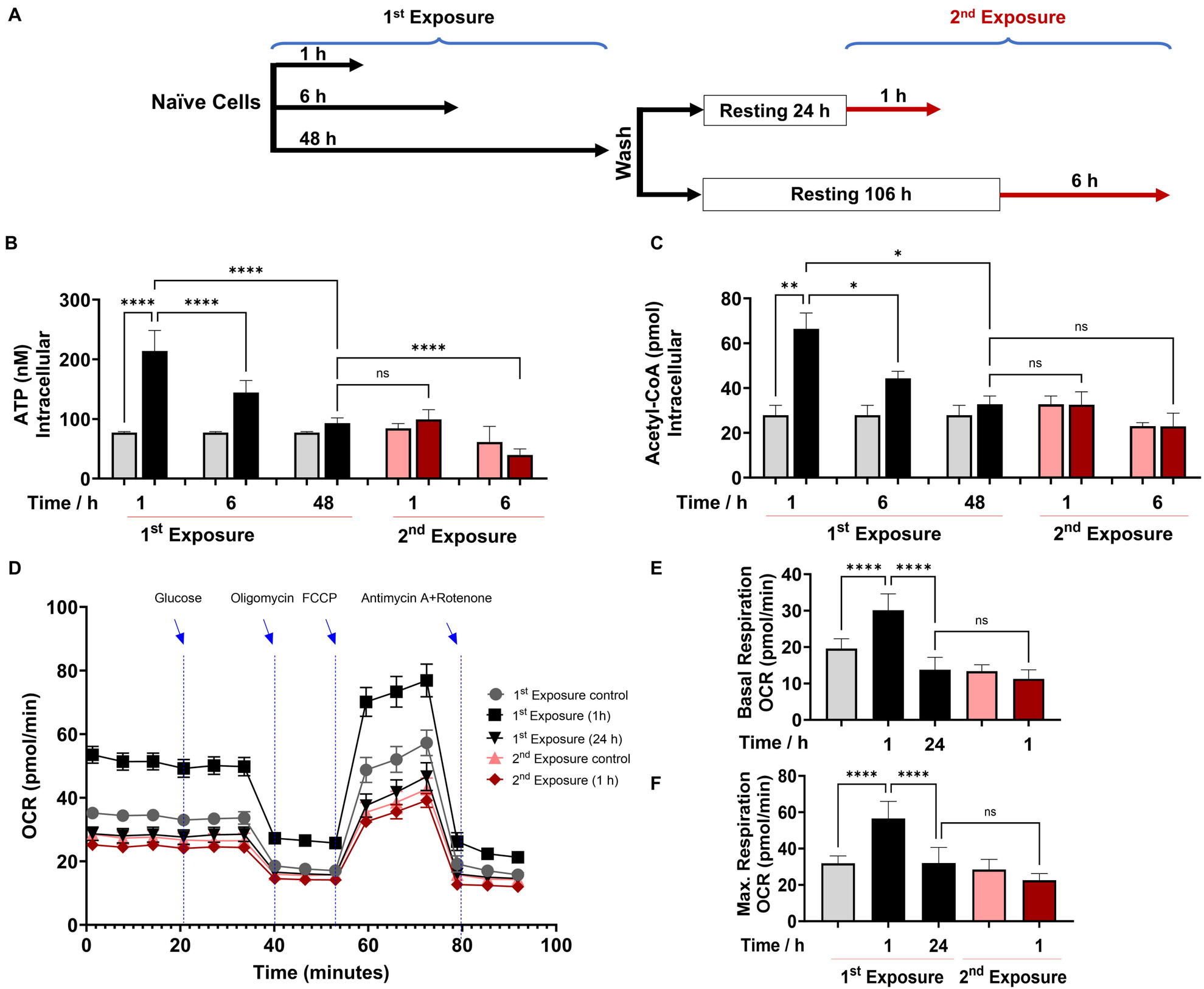
A
1st Exposure
2nd Exposure
Naïve Cells
1 h
6 h
48 h
Wash
Resting 24 h
1 h
Resting 106 h
6 h
B
ATP (nM) Intracellular
Time / h
1st Exposure
2nd Exposure
C
Acetyl-CoA (pmol) Intracellular
Time / h
1st Exposure
2nd Exposure
D
Glucose
Oligomycin
FCCP
Antimycin A+Rotenone
OCR (pmol/min)
Time (minutes)
1st Exposure control
1st Exposure (1h)
1st Exposure (24 h)
2nd Exposure control
2nd Exposure (1 h)
E
Basal Respiration OCR (pmol/min)
Time / h
F
Max. Respiration OCR (pmol/min)
Time / h
1st Exposure
2nd Exposure

Figure 1

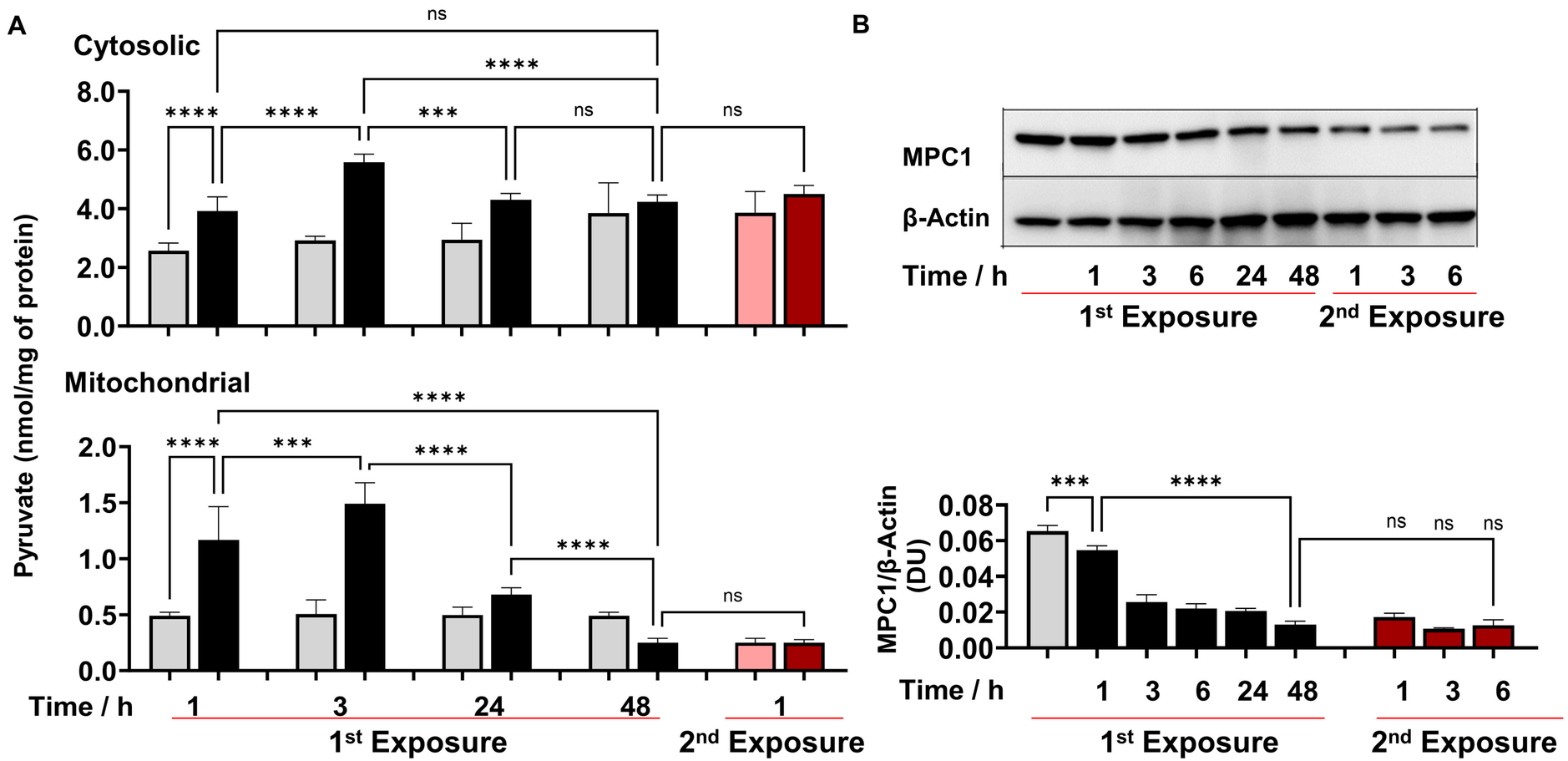
A
Cytosolic
Mitochondrial
Pyruvate (nmol/mg of protein)
8.0
6.0
4.0
2.0
0.0
1.5
1.0
0.5
****
***
ns
Time / h
1
3
24
48
1st Exposure
2nd Exposure
B
MPC1
β-Actin
Time / h
1 3 6 24 48 1 3 6
1st Exposure
2nd Exposure
MPC1/β-Actin (DU)
0.08
0.06
0.04
0.02
0.00

Figure 2

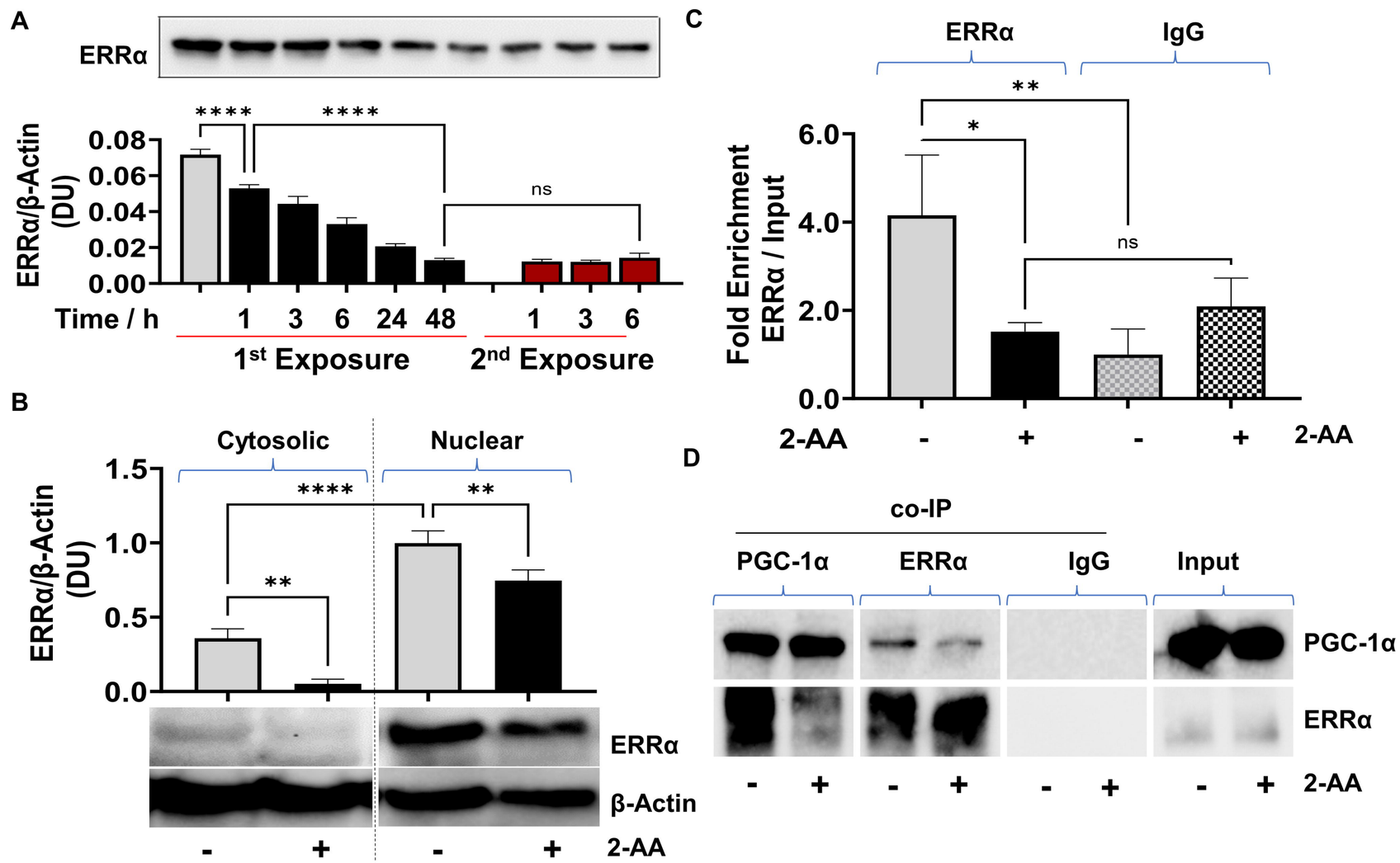
A
ERRα
ERRα/β-Actin (DU)
0.08
0.06
0.04
0.02
0.00
****
****
ns
Time / h
1
3
6
24
48
1
3
6
1st Exposure
2nd Exposure
B
Cytosolic
Nuclear
1.5
1.0
0.5
0.0
****
**
**
ERRα
β-Actin
-
+
-
+
2-AA
C
ERRα
IgG
Fold Enrichment ERRα / Input
6.0
4.0
2.0
0.0
**
*
ns
2-AA
-
+
-
+
2-AA
D
co-IP
PGC-1α
ERRα
IgG
Input
PGC-1α
ERRα
-
+
-
+
-
+
-
+
2-AA

Figure 3

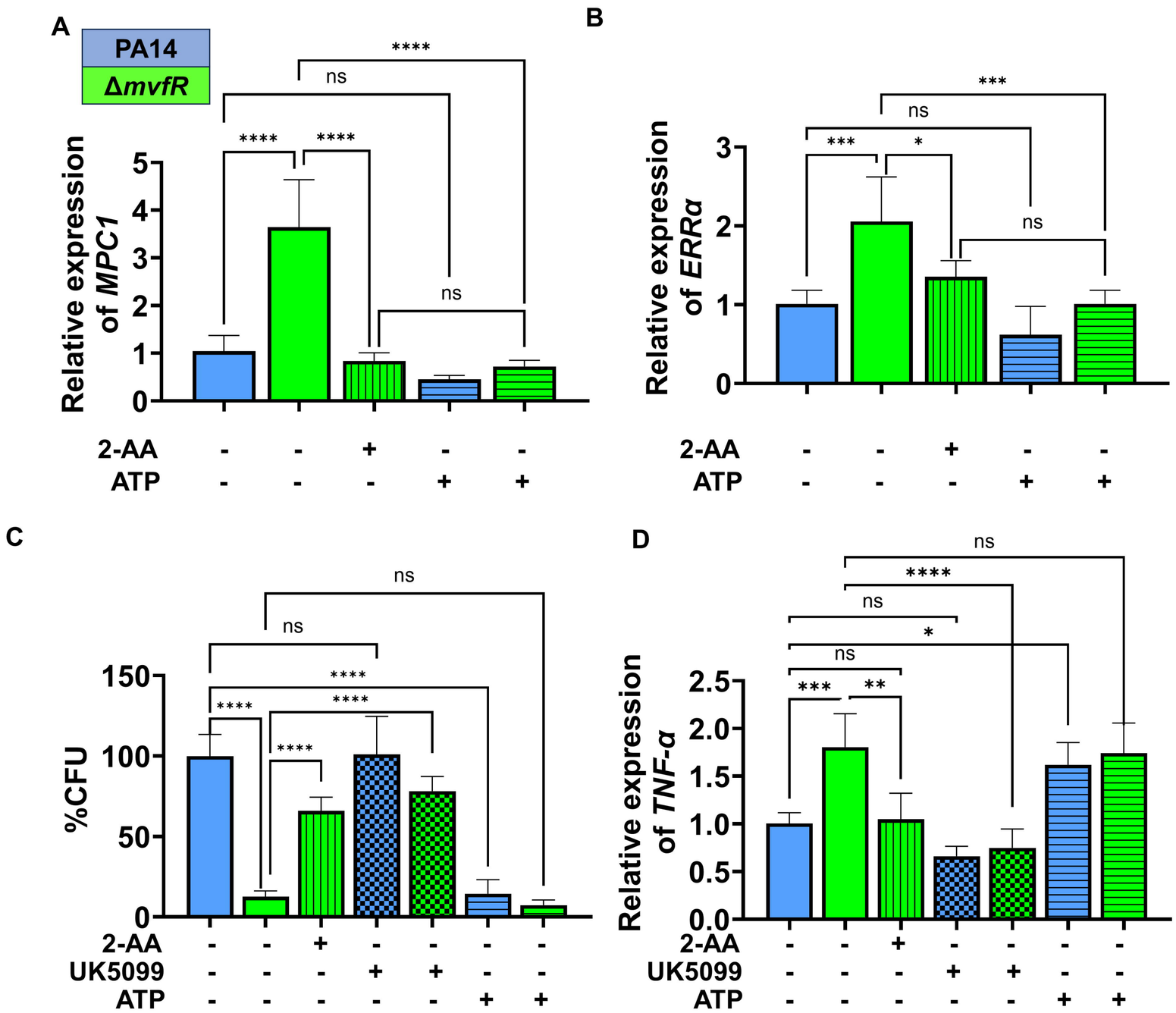
A
PA14
ΔmvfR
Relative expression of MPC1
2-AA
ATP
B
Relative expression of ERRα
2-AA
ATP
C
%CFU
2-AA
UK5099
ATP
D
Relative expression of TNF-α
2-AA
UK5099
ATP

Figure 4

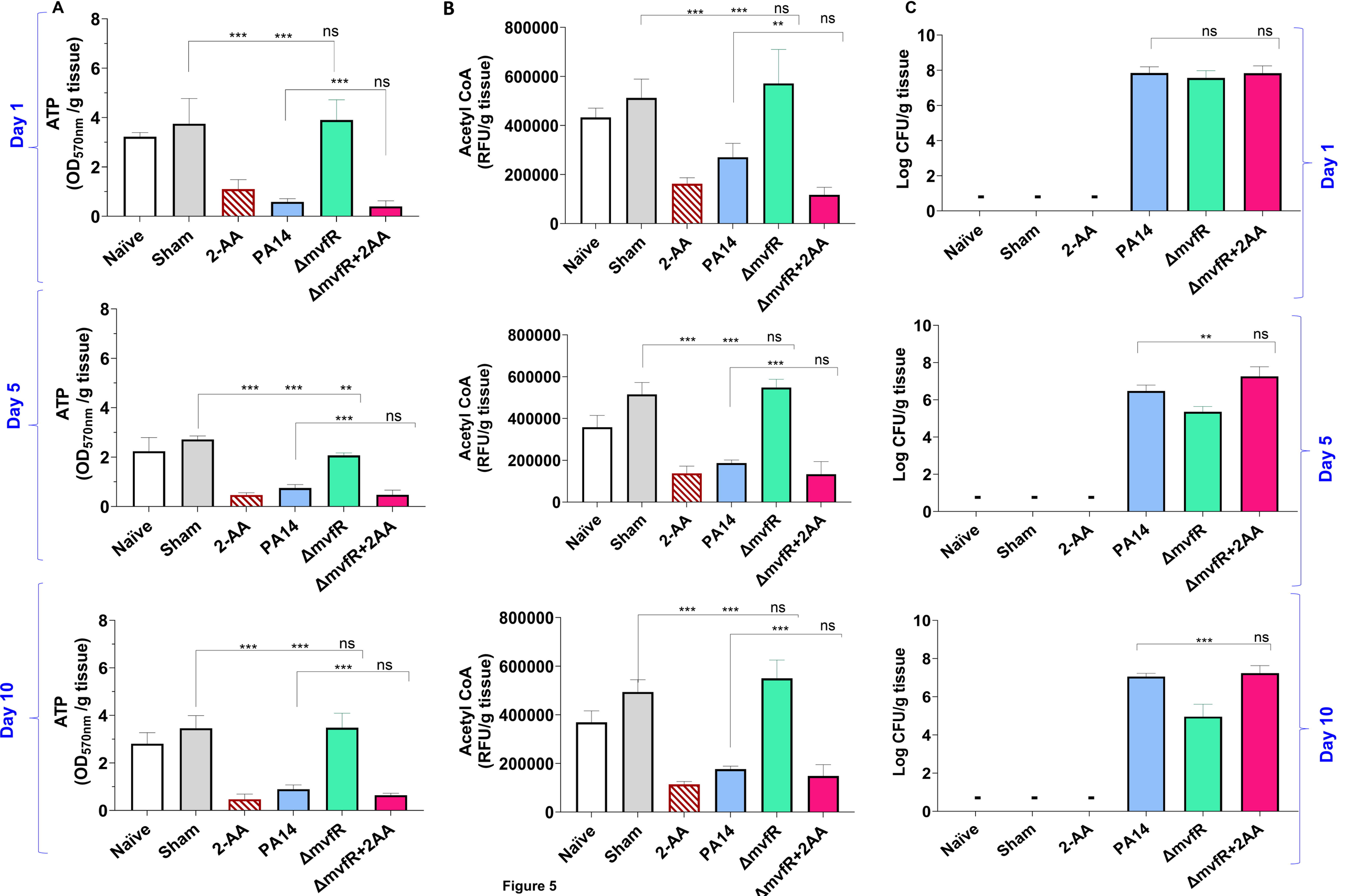
A
B
C
Day 1
Day 5
Day 10
ATP
(OD570nm /g tissue)
Acetyl CoA
(RFU/g tissue)
Log CFU/g tissue
Naïve
Sham
2-AA
PA14
ΔmvfR
ΔmvfR+2AA
***
**
ns

Figure 5

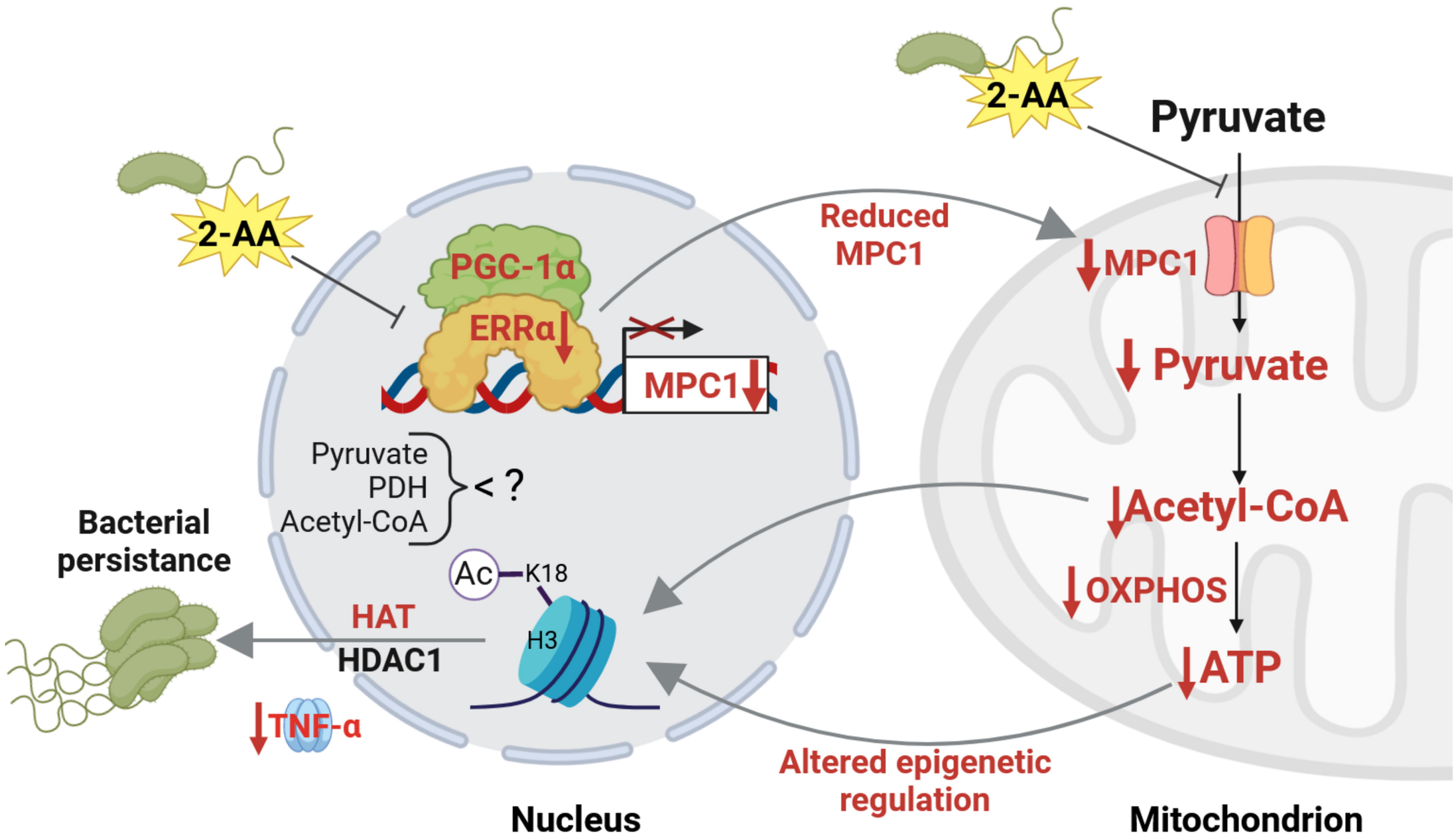
2-AA
2-AA
Pyruvate
Reduced
MPC1
PGC-1α
ERRα
MPC1
MPC1
Pyruvate
Pyruvate
PDH
Acetyl-CoA
< ?
Acetyl-CoA
Bacterial
persistance
Ac
K18
OXPHOS
HAT
H3
HDAC1
ATP
TNF-α
Altered epigenetic
regulation
Nucleus
Mitochondrion

Figure 6

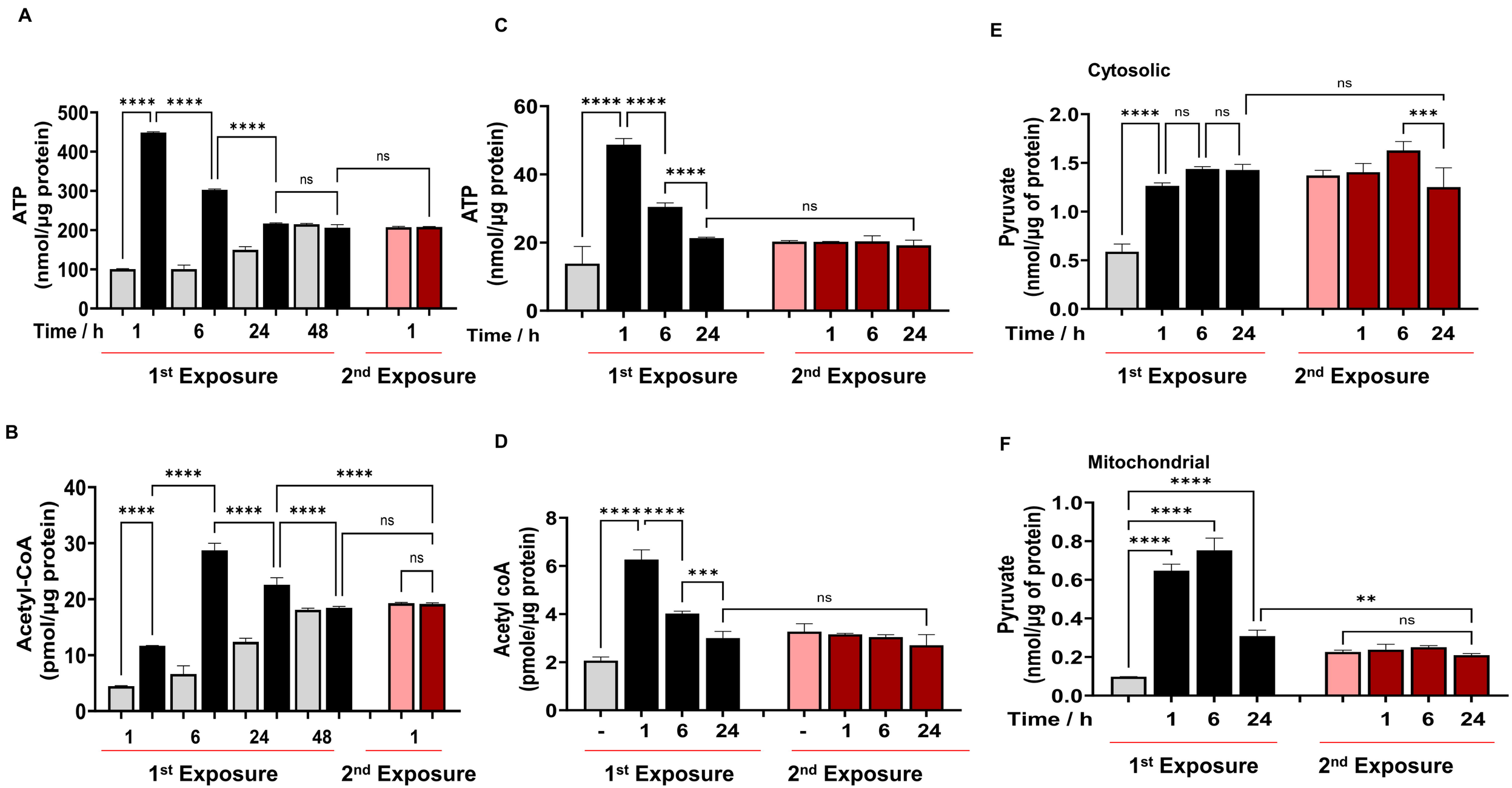
A
ATP (nmol/µg protein)
Time / h
1st Exposure
2nd Exposure
B
Acetyl-CoA (pmol/µg protein)
C
ATP (nmol/µg protein)
D
Acetyl coA (pmole/µg protein)
E
Cytosolic
Pyruvate (nmol/µg of protein)
F
Mitochondrial
Pyruvate (nmol/µg of protein)

Figure S1

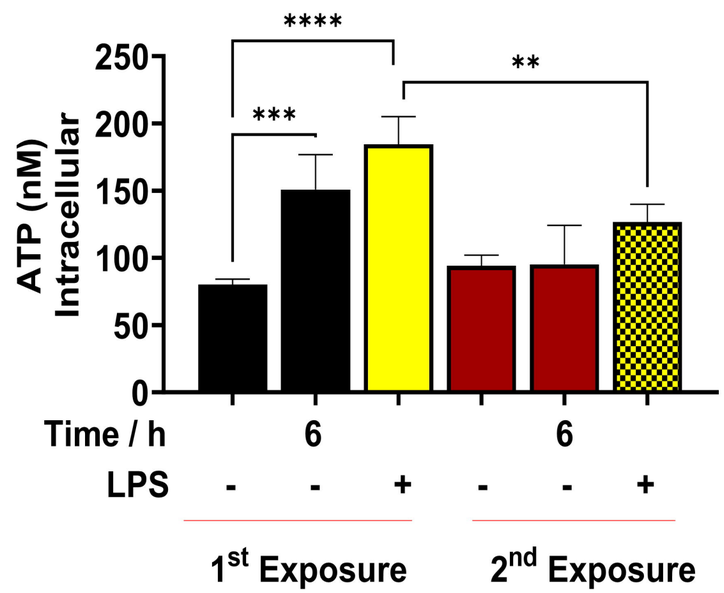
****
**
***
ATP (nM)
Intracellular
250
200
150
100
50
0
Time / h
6
6
LPS
-
-
+
-
-
+
1st Exposure
2nd Exposure

Figure S2

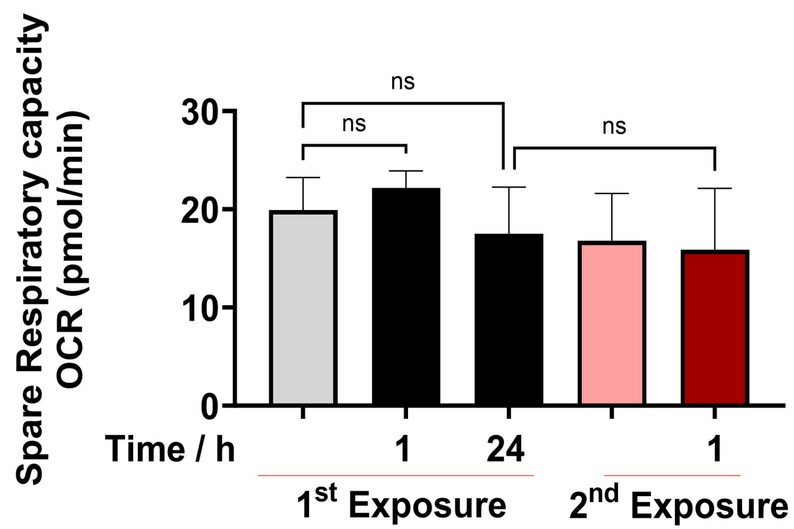
Spare Respiratory capacity
OCR (pmol/min)
30
20
10
0
ns
ns
ns
Time / h
1
24
1
1st Exposure
2nd Exposure

Figure S3